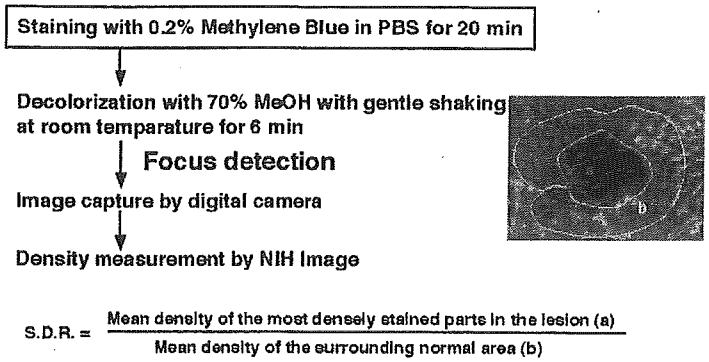

Fig. 1. Experimental procedures for the differential staining method and for analysis of digitized images of ACF. ACF were stained with 0.2% methylene blue in phosphate-buffered saline for 20 min, and then decolorized by being submerged in 70% methanol with gentle shaking at room temperature for 6 min. The staining signal intensity of each lesion was then calculated as follows. Mean densities of the most densely stained region in the ACF (area 'a'), usually composed of a limited number of crypts, and the surrounding normal portion of the colon (area 'b') were measured, and the signal density ratio (S.D.R.) between ACF and the surrounding normal area was calculated according to the formula.

2.5. Quantification of signal intensity of ACF staining

Analysis of the digitized image of each ACF was performed on a Macintosh computer using the public domain NIH Image program (developed at the US National Institutes of Health and available on the Internet at http://rsb.info.nih.gov/nih-image/). Briefly, mean signal densities of ACF and the surrounding normal area for each were measured and the signal density ratio (S.D.R.) then calculated according to the formula: 'S.D.R.=Mean density of ACF/mean density of the surrounding normal colon mucosa' (Fig. 1). When an ACF was composed of heterogeneous crypts, the most densely stained parts, which are usually composed of a few crypts, were subjected to analysis.

2.6. Histological analysis of ACF and colon tumors

ACF identified by the differential staining method were resected along with surrounding normal colon tissues with a razor blade as 2 mm widths of transverse sections under microscopic observation, and embedded in paraffin blocks. Histological diagnosis and grading of lesions were made by a trained pathologist (M.W.), who was blind to both experimental protocols and the S.D.R. values. Alcian Blue (pH 2.5)/periodic acid–Schiff base (AB–PAS) staining was also carried out to evaluate the status of goblet cells in crypts, as described elsewhere [19]. Histological analysis of colon tumors was carried out according to the intestinal tumor classification in the rat as previously reported [13].

2.7. Immunohistochemical analysis of β-catenin and Ki-67 antigen

Paraffin sections of ACF prepared at 3.5 μm thickness were stained with a mouse anti-β-catenin antibody (BD Transduction Laboratory, Lexington, KY) and a rabbit polyclonal antibody (Novacastra Laboratory, Newcastle upon Tyne, UK) as described previously [13].

2.8. Statistical analysis

All statistical analyses were performed by the Kruskal–Wallis test using SPSS for Macintosh (SPSS, Inc., Tokyo, Japan). Significance was concluded with a P-value of 0.05.

3. Results

3.1. Detection of conventional ACF by methylene blue staining

Conventional ACF were easily visualized by staining with 0.2% methylene blue, being slightly elevated above the surrounding mucosa and

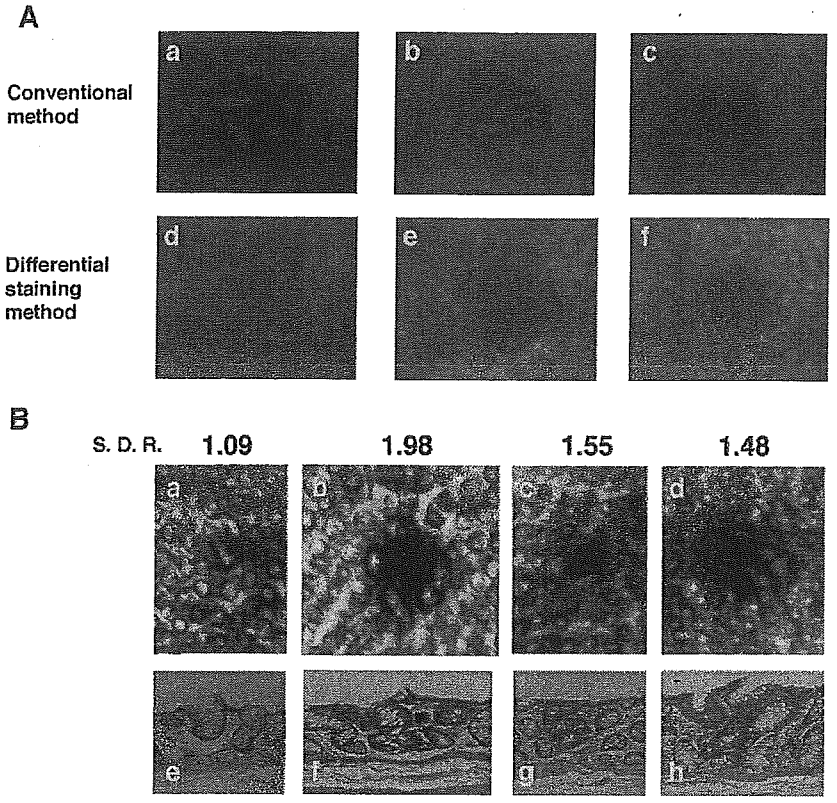

Fig. 2. (A) Representative features of ACF. (a–c) ACF detected by the conventional methylene blue staining (×40 magnification). (d–f) ACF detected by the differential staining method (×40 magnification). Lesions d, e and f are the same with a, b and c, respectively. Note that after decolorization with 70% methanol, some of the lesions became undetectable, while signals for b and c, for example, became much clearer. (B) Digitized images and signal density ratios for ACF. Digitized images of lesions detected by differential staining (a–d, ×40 magnification) and their histological features on H&E staining (e–h, ×100 magnification). Signal density ratio (S.D.R.) values are indicated at the top of the panel. (a and e) a lesion almost indistinguishable from the surrounding normal colon mucosa; (b and f) a dysplastic ACF mainly composed of dysplastic crypts; (c and g) a dysplastic ACF that became evident only after the decolorization process; (d and h) an ACF demonstrating heterogeneous histological features. The right part of the ACF in (d) and (h) is composed of non-dysplastic crypts and the left half is dysplastic.

demonstrating characteristic oval or slit-like orifices (Fig. 2A-a and b). Occasionally, some ACF were detected as almost normal-sized lesions with simply dense staining by methylene blue (Fig. 2A-c). The average number of conventional ACF induced in the PhIP-diet group was 8.0 ± 3.3 per animal, as compared to 0.6 ± 0.8 in the control group.

3.2. Detection of ACF by differential staining with methylene blue

Representative features of ACF after the differential staining method are depicted in Fig. 2A-d~f, which correspond to the same lesion as demonstrated in Fig. 2A-a~c, respectively. The numbers of ACF detected in the PhIP-diet and control groups were 7.9 ± 3.9 and 0.5 ± 0.7 per animal, respectively. Signal intensities and macroscopic appearance of ACF did not change significantly by changing the duration of the decolorization process from 4 to 6 min (unpublished data). Although the numbers of detected ACF were almost equivalent to those observed using the conventional method, a few of the lesions became undetectable and some new ACF became evident because of the increased contrast from surrounding normal crypts (Fig. 2A-f). The average number of newly identified ACF by this novel

Table 1
Distribution of S.D.R. values and histological diagnosis of ACF induced by PhIP

S.D.R.[a]	Histology	No. of foci
1.50≤	Dysplastic	27 (4)[b]
1.40≤, <1.50	Dysplastic	11 (1)
<1.40	Non-dysplastic	8 (0)
	Non-dysplastic	18 (0)

A total of 64 ACF collected from 10 rats were subjected to histological evaluation.
[a] S.D.R., the signal density ratio. Its definition is noted in Section 2.
[b] Numbers in parentheses indicate the number of newly identified lesions by the differential staining method.

method was 0.8±1.1 per animal in the PhIP-diet group.

3.3. Quantification of staining intensity by digitizing signal density

To verify the rationale for the differential staining method, staining intensities for individual lesions were evaluated with digital images captured by a CCD camera. Representative digitized images of lesions and S.D.R. values are demonstrated along with the H&E staining features in Fig. 2B. Lesions giving S.D.R. values close to 1.00 were almost indistinguishable from the surrounding normal tissue (Fig. 2B-a). Lesions with 1.50 or more S.D.R. contained dysplastic crypts (Fig. 2B-b/f and c/g). Occasionally, small lesions that could be barely detected by the conventional method became evident by the differential staining method (Fig. 2B-c). In addition, some lesions demonstrated heterogeneous features as, for example, represented in Fig. 2B-d. The right part of the lesion in Fig. 2B-d shows typical histological features of non-dysplastic ACF, and the left part is dysplastic (Fig. 2B-h).

3.4. Differential staining between dysplastic and non-dysplastic ACF induced by PhIP

From a group of 10 rats in PhIP-diet group, 64 ACF were collected and subjected to histological examination. A total of 26 lesions were diagnosed as non-dysplastic and the remaining 38 as dysplastic (Table 1). S.D.R. values of the non-dysplastic lesions ranged from 1.09 to 1.49, and for dysplastic ACF from 1.40 to 2.08 (Fig. 3). Four of five newly identified ACF by our differential staining method exhibited S.D.R. values of 1.50 or greater, and the remaining one 1.40. Lesions with 1.50 or greater S.D.R. were all revealed to be dysplastic. In addition, all those with an S.D.R. of less than 1.40 were non-dysplastic (Table 1). Lesions between 1.40 and 1.50 S.D.R. values were a mixture of non-dysplastic and dysplastic ACF, and approximately 30% of ACF fell within this range. All of the five newly identified lesions were diagnosed as dysplastic. Most of the dysplastic ACF demonstrated β-catenin accumulation in either the cytoplasm (Fig. 4a) or the nucleus (Fig. 4d), and showed increased cell proliferation estimated by Ki-67 antigen positive cells in the crypt (Fig. 4b and e). A substantial decrease in goblet cells and mucin production was also observed in dysplastic lesions (Fig. 4c and f).

3.5. Characteristic features of dysplastic ACF after differential staining

After the differential staining, characteristic features of dysplastic ACF are summarized as follows. Dysplastic lesions contained crypts with homogeneously dense staining, which attribute high S.D.R. values (Fig. 2B-b, c and left part of 2B-d). The orifice of the crypts was relatively small compared to the normal crypts or even undetectable. In contrast,

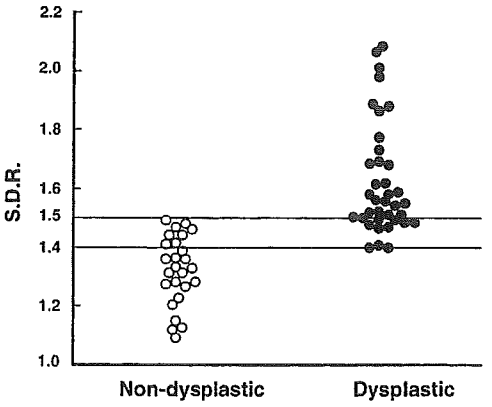

Fig. 3. Distribution of signal density ratios of non-dysplastic and dysplastic ACF. S.D.R. values of non-dysplastic ACF ranged from 1.09 to 1.49. In contrast, dysplastic ACF demonstrated much higher values, ranging from 1.40 to 2.08. Note that lesions with 1.50 or more S.D.R., and those with less than 1.40 S.D.R. were all diagnosed as dysplastic and non-dysplastic ACF, respectively. Open circles, non-dysplastic ACF; closed circles, dysplastic ACF.

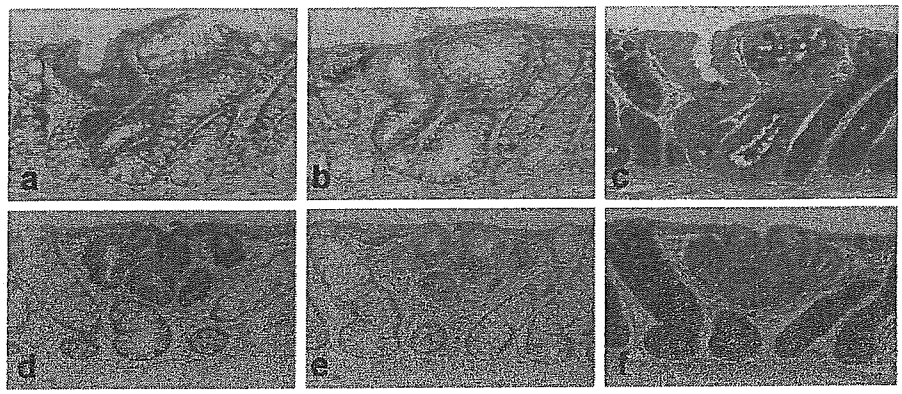

Fig. 4. Histochemical analysis of dysplastic ACF. Dysplastic ACF were subjected to immunohistochemical analysis for β-catenin (a and d) and Ki-67 antigen (b and e), and AB-PAS staining (c and f). The lesion in the upper panel (a–c) is the same ACF depicted in Fig. 2B-d with non-dysplastic (right part of the lesion) and dysplastic crypts (left part of the lesion). The lesion in the lower panel (d–f) was mostly composed of dysplastic crypts. β-Catenin accumulation in either the cytoplasm (a) or the nucleus (d) is apparent. As for Ki-67 antigen positive cells, normal crypts showed labeling cells restricted to the lower half of the crypts. In contrast, labeling cells extended into the upper portions of the dysplastic crypt (b and e). AB–PAS staining shows a substantial decrease in goblet cells and mucin production in crypts (c and f).

non-dysplastic ACF was composed of crypts with clear orifices, either split- or round-shaped (Fig. 2B-a and right part of 2B-d). Using these criteria, lesions with intermediate signals (S.D.R. = 1.40–1.50) could be satisfactorily sub-grouped into non-dysplastic and dysplastic ACF without conducting a laborious histological examination (unpublished data).

3.6. Comparisons of induction of ACF, dysplastic ACF and colon tumors for the three HCAs

The numbers of conventional ACF, ACF detected by the novel differential staining method, and dysplastic ACF, induced by PhIP, MeIQ and IQ at experimental week 32 were shown in Table 2. Dysplastic ACF were judged from the characteristic appearance without conducting histology. It is of great importance to note that the number of colon tumors, either adenomas or adenocarcinomas, detected at week 32 was almost equivalent for PhIP and MeIQ, and that for IQ was approximately half that. These values demonstrated far superior correlation with numbers of ACF with 1.40 (or 1.50) or greater S.D.R, namely those of lesions representing dysplastic ACF, than with conventional ACF (Table 2).

4. Discussion

We have here developed an efficient method to distinguish dysplastic lesions efficiently and

Table 2
ACF, dysplastic ACF and colon tumors induced by representative HCAs

Chemical	No. of rat	Conventional ACF	ACF[a,b]				Tumor
			Total	S.D.R[c] ≥ 1.40	S.D.R ≥ 1.50	Dysplastic ACF[d]	
PhIP	20	8.0 ± 3.3	7.9 ± 3.9 (0.8 ± 1.1)	4.3 ± 2.9 (0.7 ± 1.0)	2.5 ± 2.1 (0.4 ± 0.6)	3.2 ± 2.6 (0.5 ± 0.7)[e]	0.7 ± 0.9
MeIQ	18	15.4 ± 4.7	11.9 ± 3.4 (0.8 ± 0.9)	4.8 ± 2.1 (0.4 ± 0.6)	2.1 ± 1.8 (0.1 ± 0.3)	3.1 ± 2.2 (0.4 ± 0.5)	0.6 ± 0.8
IQ	19	4.9 ± 1.7	4.9 ± 2.1 (1.0 ± 0.9)	2.7 ± 1.4 (0.6 ± 0.8)	1.4 ± 1.3 (0.2 ± 0.5)	2.0 ± 1.6 (0.5 ± 0.8)	0.3 ± 0.6

[a] ACF detected by the differential staining method.
[b] The numbers in parentheses indicate newly identified lesions.
[c] S.D.R., the signal density ratio. Its definition is noted in Section 2.
[d] The numbers of dysplastic ACF were evaluated judging from the characteristic features of the lesions without H&E examination.
[e] The dysplastic ACF induced by PhIP include 64 lesions which were subjected to histological analysis. Thirty-eight lesions were confirmed histologically as being dysplastic.

selectively among a large number of ACF. Using this differential staining method, PhIP-induced lesions that gave high staining signals (S.D.R. $\geqq$ 1.50) were all diagnosed as dysplastic. In contrast, those with low signals (S.D.R. $<$ 1.40) were diagnosed as non-dysplastic. The dysplastic lesions frequently demonstrated accumulation of β-catenin, and a decrease or loss of goblet cells, and a subset also harbored β-catenin mutations (unpublished data), as described in our previous study [13].

At present, although we do not have a definitive explanation of how the decolorization process provides differential staining of dysplastic and non-dysplastic lesions, a simple explanation can be made on the basis of methylene blue capture by DNA [20]. Lesions composed of a large number of cells and/or high density of cells with enlarged nuclei and/or nuclear stratification, characteristic of dysplasia, might be expected to be more resistant to decolorization by methanol treatment than normal crypts or non-dysplastic lesions.

As mentioned above, it would be of great assistance to researchers if dysplastic ACF could be diagnosed with accuracy without conducting a histological examination. Furthermore, the presence of histologically heterogeneous components in dysplastic ACF might also be identified by the differential staining method as exemplified in Fig. 2B-d. Dysplastic ACF could thus be diagnosed at more than 90% sensitivity without the necessity for a laborious and time-consuming preparation of histological sections. This novel method could also be extended for analysis of lesions induced by AOM. From our preliminary study, the majority of AOM-induced ACF could be classified as non-dysplastic ACF by this differential staining method (unpublished data). More detailed histological analysis is currently ongoing to validate the relevance of this method for AOM-induced lesions as well.

From the present experiments using representative HCAs, total numbers of ACF detected by our novel method more closely correlate with induction of tumors as compared with those observed with the conventional approach. In addition, it would appear that lesions induced by MeIQ under the current condition (300 ppm in diet) might more preferentially be non-dysplastic than those due to PhIP or IQ. In conclusion, our findings indicate that differentially stained dysplastic ACF are particularly relevant as surrogate endpoint markers for colon carcinogenesis induced by heterocyclic amines, providing us with a powerful tool for investigation of carcinogenicity and chemoprevention using animal models.

Acknowledgements

This work was supported in part by a Grant-in-Aid for the Second Term of the Comprehensive 10-Year Strategy for Cancer Control from the Ministry of Health, Labour and Welfare of Japan, and a Grant-in-Aid for Cancer Research from the Ministry of Health, Labour and Welfare of Japan.

References

[1] W.F. Dove, R.T. Cormier, K.A. Gould, R.B. Halberg, A.J. Merritt, M.A. Newton, A.R. Shoemaker, The intestinal epithelium and its neoplasms: genetic, cellular and tissue interactions, Philos. Trans. R. Soc. Lond. B Biol. Sci. 353 (1998) 915–923.

[2] M. Nagao, T. Ushijima, M. Toyota, R. Inoue, T. Sugimura, Genetic changes induced by heterocyclic amines, Mutat. Res. 376 (1997) 161–167.

[3] R.P. Bird, Observation and quantification of aberrant crypts in the murine colon treated with a colon carcinogen: preliminary findings, Cancer Lett. 37 (1987) 147–151.

[4] D.E. Corpet, S. Tache, Most effective colon cancer chemopreventive agents in rats: a systematic review of aberrant crypt foci and tumor data, ranked by potency, Nutr. Cancer 43 (2002) 1–21.

[5] M. Takahashi, M. Fukutake, T. Isoi, K. Fukuda, H. Sato, K. Yazawa, et al., Suppression of azoxymethane-induced rat colon carcinoma development by a fish oil component, docosahexaenoic acid (DHA), Carcinogenesis 18 (1997) 1337–1342.

[6] S. Takahashi, K. Ogawa, H. Ohshima, H. Esumi, N. Ito, T. Sugimura, Induction of aberrant crypt foci in the large intestine of F344 rats by oral administration of 2-amino-1-methyl-6-phenylimidazo[4,5-*b*]pyridine, Jpn. J. Cancer Res. 82 (1991) 135–137.

[7] M. Ochiai, H. Nakagama, M. Watanabe, Y. Ishiguro, T. Sugimura, M. Nagao, Efficient method for rapid induction of aberrant crypt foci in rats with 2-amino-1-methyl-6-phenylimidazo[4,5-*b*]pyridine, Jpn. J. Cancer Res. 87 (1996) 1029–1033.

[8] N. Ito, R. Hasegawa, M. Sano, S. Tamano, H. Esumi, S. Takayama, T. Sugimura, A new colon and mammary carcinogen in cooked food, 2-amino-1-methyl-6-phenylimidazo[4,5-*b*]pyridine (PhIP), Carcinogenesis 12 (1991) 1503–1506.

[9] R. Hasegawa, M. Sano, S. Tamano, K. Imaida, T. Shirai, M. Nagao, et al., Dose-dependence of 2-amino-1-methyl-6-phenylimidazo[4,5-*b*]pyridine (PhIP) carcinogenicity in rats, Carcinogenesis 14 (1993) 2553–2557.

[10] Y. Zheng, P.M. Kramer, R.A. Lubet, V.E. Steele, G.J. Kelloff, M.A. Pereira, Effect of retinoids on AOM-induced colon cancer in rats: modulation of cell proliferation, apoptosis and aberrant crypt foci, Carcinogenesis 20 (1999) 255–260.

[11] M.A. Pereira, L.H. Barnes, V.L. Rassman, G.V. Kelloff, V.E. Steele, Use of azoxymethane-induced foci of aberrant crypts in rat colon to identify potential cancer chemopreventive agents, Carcinogenesis 15 (1994) 1049–1054.

[12] C.V. Rao, C.-X. Wang, B. Simi, R. Lubet, G. Kelloff, V. Steele, B.S. Reddy, Enhancement of experimental colon cancer by genistein, Cancer Res. 57 (1997) 3717–3722.

[13] M. Ochiai, M. Ushigome, K. Fujiwara, T. Ubagai, T. Kawamori, T. Sugimura, et al., Characterization of dysplastic aberrant crypt foci in the rat colon induced by 2-amino-1-methyl-6-phenylimidazo[4,5-*b*]pyridine, Am. J. Pathol. 163 (2003) 1607–1614.

[14] M. Takahashi, K. Wakabayashi, Gene mutations and altered gene expression in azoxymethane-induced colon carcinogenesis in rodents, Cancer Sci. 95 (2004) 475–480.

[15] Y. Yamada, H. Mori, Pre-cancerous lesions for colorectal cancers in rodents: a new concept, Carcinogenesis 24 (2003) 1015–1019.

[16] G. Caderni, A.P. Femia, A. Giannini, A. Favuzza, C. Luceri, M. Salvadori, P. Dolara, Identification of mucin-depleted foci in the unsectioned colon of azoxymethane-treated rats: correlation with carcinogenesis, Cancer Res. 63 (2003) 2388–2392.

[17] J.E. Paulsen, I.-L. Steffensen, E.M. Loberg, T. Husoy, E. Namork, J. Alexander, Qualitative and quantitative relationship betweeen dysplastic aberrant crypt foci and tumorigenesis in the *Min*/+ mouse colon, Cancer Res. 61 (2001) 5010–5015.

[18] H. Ohgaki, S. Takayama, T. Sugimura, Carcinogenicities of heterocyclic amines in cooked food, Mutat. Res. 259 (1991) 399–410.

[19] K. Fujiwara, M. Ochiai, T. Ohta, M. Ohki, H. Aburatani, M. Nagao, et al., Global gene expression analysis of rat colon cancers induced by a food-borne carcinogen, 2-amino-1-methyl-6-phenylimidazo[4,5-*b*]pyridine, Carcinogenesis 25 (2004) 1495–1505.

[20] D.E. Comings, E. Avelino, Mechanisms of chromosome banding. VII. Interaction of methylene blue with DNA and chromatin, Chromosoma 51 (1975) 365–379.

Review Article

Modeling human colon cancer in rodents using a food-borne carcinogen, PhIP

Hitoshi Nakagama,[1] Masako Nakanishi and Masako Ochiai

Biochemistry Division, National Cancer Center Research Institute,1-1 Tsukiji, 5-chome, Chuo-ku, Tokyo 104-0045, Japan

(Received May 18, 2005/Revised August 1, 2005/Accepted August 3, 2005/Online publication October 3, 2005)

Animal models provide researchers with powerful tools to elucidate multistage mechanisms for cancer development and to gain further insights into the biological roles of various cancer-related genes in *in vivo* situations. As for colon cancer models in rodents, *Apc*-disrupted mice, including Apc^{Min}, have been one of the most widely utilized animal models to dissect the molecular events implicated in the development of intestinal tumors. In rats, several models have been established using chemical carcinogens, including azoxymethane and 2-amino-1-methyl-6-phenylimidazo-[4,5-*b*]pyridine (PhIP). The former is a representative colon carcinogenic alkylating agent, and the latter a heterocyclic amine produced while cooking meat and fish, which people are exposed to in ordinary life. It is of great importance to note that PhIP preferentially targets the colon and prostate gland in male rats, and the mammary glands in female rats. Cancers in these three organs are common in Western countries and are currently increasing in Japan, where modern dietary habits are rapidly becoming more like those of the West. In the present article, the history of PhIP-induced colon cancer models in rodents, activation/detoxification mechanisms of PhIP with regard to the formation of PhIP-DNA adducts, mechanistic approaches to dissect the molecular events involved in the development of colon cancer by PhIP, and epidemiological evidence of human exposure to PhIP are overviewed. The induction of Paneth cell maturation/differentiation in PhIP-induced colon cancers, genetic traits affecting susceptibility to colon carcinogenesis, and the biological relevance of colon cancer models in rodents to studying human colon carcinogenesis are also discussed. (*Cancer Sci* 2005; 96: 627–636)

Human cancers are believed to be caused by the combined effects of both hereditary and environmental factors. Recently, Lichtenstein *et al.* published an important work that estimated the effects of genetic and environmental factors on common cancers using data from the Swedish, Danish and Finnish twin registries.[1]

Regarding hereditary factors, a considerable amount of research into familial cancers has revealed a series of tumor suppressor genes, including *TP53*, *RB*, *APC*, *BRCA1/2*, *TSC1/2*, *WT1* and *PTEN*, comprising genetic traits with high-penetrance. However, we should also take low-penetrance genetic traits, for example genes in the *CYP*, *NAT* and *GST* families, into consideration. As for environmental factors, epidemiological studies have shown that smoking, infection and dietary habits play an important role in the development of sporadic human cancers.[2] Regarding human cancers related to infection and/or inflammation, examples are hepatitis B and C viruses in hepatocellular carcinoma, *Helicobacter pylori* in gastric cancer, and human papilloma virus in cervical cancer,[3] although molecular mechanisms underlying the onset of infection-related cancers still remain elusive. As for dietary factors, they are estimated to account for approximately one-third of human cancers.[2]

Concerning daily food intake, nitrites/nitrates may play some roles in relation to the formation of nitroso compounds, but the significance of nitroso compounds in human carcinogenesis is still unclear. Other important compounds in cooked foods are polycyclic aromatic hydrocarbons[4] and heterocyclic amine (HCA) compounds.[5,6] An example of the former is, for instance, benzo[*a*]pyren (B[*a*]P), which is present in roasted coffee beans.[4] HCA compounds are some of the most abundant genotoxic mutagens present in our environment, and humans are exposed to them in ordinary daily life. In this review article, the research history of 2-amino-1-methyl-6-phenylimidazo[4,5-*b*]pyridine (PhIP) (one of the most abundant HCA in heated meat and fish[7]) and a colon cancer model in rodents induced by PhIP are discussed from the viewpoint of their relevance to modeling human colon cancers.

PhIP, a food-borne carcinogen

Since the first discovery of HCA in 1977,[8] tremendous progress has since been made in this field in basic research. HCA in cooked food are produced by heating amino acids and proteins, and most HCA in food are really derived from heating meat. Heating meat yields various potent imidazoquinoline, imidazoquinoxaline and imidazopyridine compounds, and they are highly mutagenic towards some strains of *Salmonella typhimurium*. Some HCA have been synthesized in abundance, and have been found to be carcinogenic in long-term animal assays. PhIP was isolated by James Felton (Lawrence Livermore National Laboratory, California) by carefully examining a fraction with low peak mutagenicity.[7] Although the specific mutagenicity of PhIP is

[1]To whom correspondence should be addressed. E-mail: hnakagam@gan2.res.ncc.go.jp
Abbreviations: AB-PAS, alcian blue-periodic acid Schiff; ACF, aberrant crypt foci; BCAC, β-catenin accumulated crypts; HCA, heterocyclic amine; MDF, mucin-depleted foci; PhIP, 2-amino-1-methyl-6-phenylimidazo[4,5-*b*]pyridine.

 doi: 10.1111/j.1349-7006.2005.00107.x

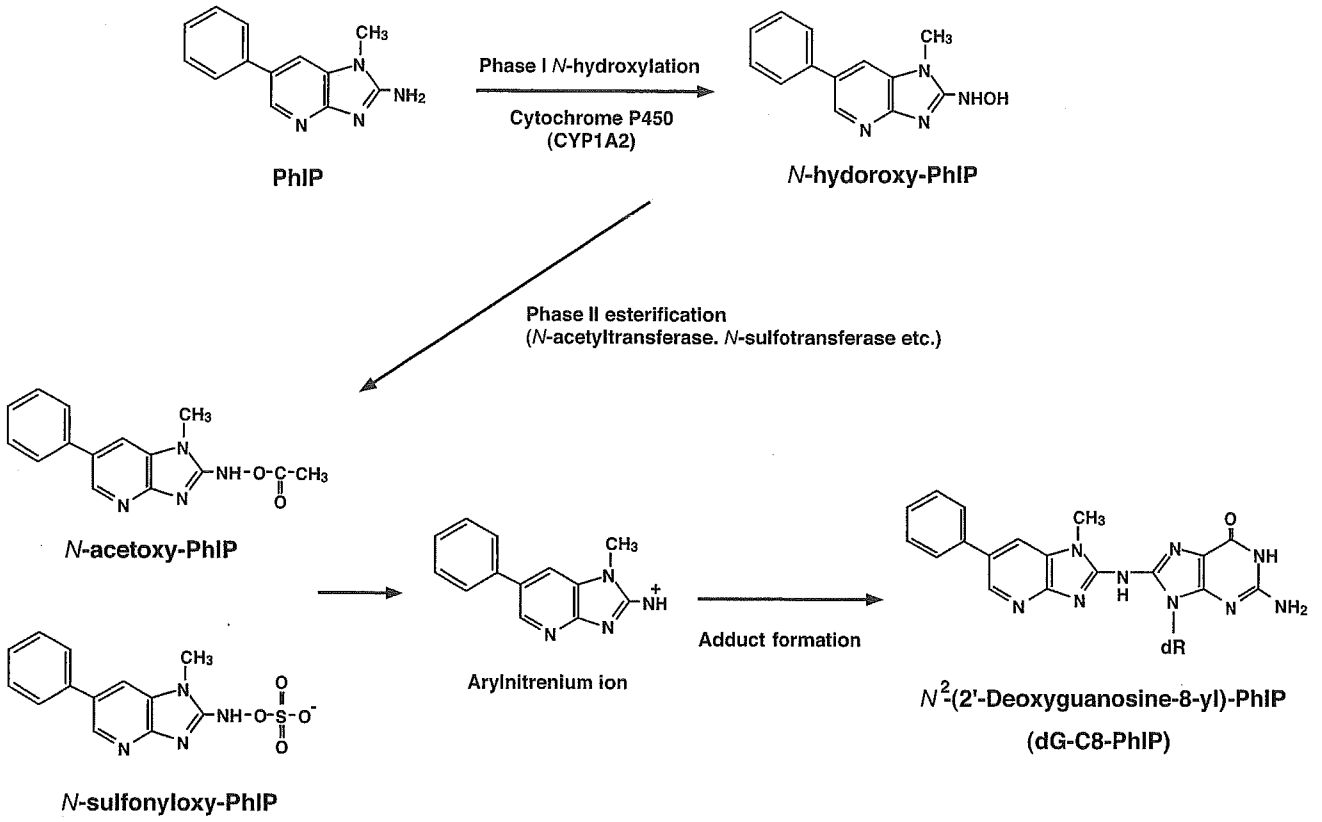

Fig. 1. Chemical structure and pathway of metabolic activation of PhIP leading to DNA adduct formation. *N*-Hydroxylation of PhIP is catalyzed by phase I hepatic cytochrome P450, mainly by CYP1A2, followed by phase II esterification with *N*-acetyltransferase and *N*-sulfotransferase. Arylnitrenium ions generated from *N*-acetoxy-PhIP or *N*-sulfonyloxy-PhIP react with nucleophilic sites in DNA, mainly at guanine bases, leading to the formation of dG-C8-PhIP adducts.

100-fold less than that of IQ and MeIQ compounds, the PhIP content in cooked meat is much higher than that of the other two compounds.[9]

Metabolic activation and detoxification of PhIP

The structure of PhIP was determined with data from mass- and nuclear magnetic resonance spectrometries as depicted in Figure 1.[7] PhIP is soluble in dimethyl sulfoxide, stable under moderately acidic and alkaline conditions, and also under dry and cold conditions for a year. Once PhIP is given to animals, it is absorbed from the alimentary tract and is immediately and widely distributed throughout the body. PhIP is then metabolically activated by Phase I and Phase II enzymes mainly in the liver, similar to other HCA compounds, and probably in terminal target organs as well.[9,10] The principal pathway for metabolic activation of PhIP is shown in Figure 1. Cytochrome P450-mediated *N*-hydroxylation of PhIP occurs predominantly by CYP1A2 at liver microsomes.[9,10] *N*-Hydroxylated metabolites of PhIP are able to bind covalently to DNA to form adducts, but are further activated by Phase II enzymes, namely *N*- and *O*-acetyltransferases (NAT1 and NAT2) and sulfotransferases (SULT), to generate carcinogenic species. The Phase II enzymes add *N*-acetoxy or *N*-sulfonyl moieties to *N*-hydroxylated PhIP in the liver and partly in the terminal target organs, and arylnitrenium ions (R-NH+) derived from these ultimate metabolites of PhIP react with DNA to generate PhIP-adducted bases,[10] which results in the induction of mutations in the DNA replication process.

As for a DNA-adduct of PhIP, the adduct in which the exocyclic amino group of PhIP covalently binds to the C8 atom of the guanine base (dG-C8-PhIP) is the major one found in calf thymus DNA reacted *in vitro* with *N*-acetoxy-PhIP,[9,10] and that found in DNA from rats exposed to PhIP. Regarding detoxification of PhIP, glutathione (GSH) and glutathione transferases (GST) play a key role. Furthermore, detoxification of *N*-hydroxylated PhIP occurs in the liver by generating glucuronate conjugates.[11] In this case, glucuronate-conjugated PhIP is secreted in the bile, deconjugated by gut flora, and reabsorbed from the gut (so-called 'enterohepatic circulation'). This circulation makes colon epithelial cells receive repeated exposure to activated PhIP *in vivo*.

Evidence of human exposure to PhIP

The amounts of PhIP in cooked meat and fish range from 0.29 to 182 ng/g,[9] and the daily intake of PhIP is estimated to range between 0 and 865 ng/day, with a mean value of 72 ng/day.[12] To date, a considerable number of reports on the presence of low levels of both PhIP and PhIP-DNA adducts in human materials such as urine, feces and hair,

 doi: 10.1111/j.1349-7006.2005.00107.x

have also been made. As for the levels of human exposure to PhIP, high performance liquid chromatography (HPLC) is able to directly and sensitively measure the PhIP in tissues at nanogram levels, and mass spectrometry (MS) gave a much higher sensitivity. Hashimoto *et al.* recently developed a column-switching liquid chromatography (LC)/MS method for quantification of PhIP in human hair samples, whose limit of quantification was 50 pg/g.[13] Using this method, PhIP at concentrations of 110–3878 pg/g was found in 42 of 46 (91.3%) hair samples from 23 healthy volunteers.[13]

Quantification of the levels of human exposure to PhIP can also be done by measuring the amount of PhIP-DNA adducts in tissue. A major DNA adduct of PhIP is dG-C8-PhIP, as described earlier, and ^{32}P-postlabeling analysis,[14] HPLC[15] and an immunohistochemical method using an anti-PhIP-adducted DNA polyclonal antibody,[16] have been widely used for the detection of PhIP-adducted DNA. Gas chromatography (GC)/MS[17] and accelerator MS (AMS)[18] analyses have also been developed to detect a tiny amount of PhIP-DNA adducts, at sensitivities in the order of 10^{-8} and 10^{-12}, respectively. PhIP-adducts detected in human colon samples by using the ^{32}P-postlabeling method are approximately three adducts per 10^8 nucleotides.[17]

Mutagenic activity of PhIP

The mutagenic activity of HCA, which has been measured using a *S. typhimurium* histidine auxotroph, varies widely among various kinds of HCA molecules (Table 1). The mutagenicity of 2-amino-3-methyl-9*H*-pyrido[2,3-*b*]indole (MeAαC) in *S. typhimurium* TA98 that detects mutants with frameshift-type mutations gave as little as 200 revertants/μg compound. 2-Amino-3-methylimidazo[4,5-*f*]quinoline (MeIQ), in contrast, gave more than 6×10^5 revertants/μg. In *S. typhimurium* TA100, which detects mutants with base substitution-type mutations, the mutagenicity of HCA range from 20 revertants/μg for 2-amino-9*H*-pyrido[2,3-*b*]indole (AαC) to 3×10^4 revertants/μg for MeIQ. As for PhIP, it produced relatively low mutagenic activities relative to other HCA: 1800 in TA98 and 120 in TA100.[9] The mutagenicity of PhIP toward mammalian cells has also been evaluated using the *Hprt* or the *Ef-2* genes as shuttle vectors. The mutant frequency of the *Hprt* gene in Chinese hamster fibroblast cells was approximately 90×10^{-6} with 100 μM PhIP, compared with 8×10^{-6} in the solvent control.[19]

In vivo mutation spectra for PhIP have been measured in various organs using Big Blue rats[20,21] and mice,[22] *gpt*Δ transgenic mice[23] and Muta mice,[24,25] and the values are summarized in Table 2. In the colon mucosa, a G-deletion is observed at a frequency of 26% and 34% in Big Blue mice and rats, respectively, and, especially, that from the 5′-GGGA-3′ sequence is somehow characteristic for PhIP. This accounts for 6.9% and 8.5% of the total mutations in the transgenic *lacI* gene in rats[20,21] and mice,[22] respectively, and 10% of all mutations detected in the *Hprt* gene in the Chinese hamster fibroblast as well.[19] As for base substitution-type mutations, G:C to T:A is the most common and accounts for approximately 25–50% of all mutations detected in the *lacI* gene of Big Blue animals.[20–22]

Table 1. Common abbreviations, full names and mutagenicity of various HCA in *Salmonella typhimurium* TA98 and TA100 with S9 mix[9]

Compound		Revertants/μg	
Abbreviation	Full name	TA98	TA100
IQ	2-amino-3-methylimidazo[4,5-*f*]quinoline	433 000	7000
IQx	2-amino-3,4-dimethylimidazo[4,5-*f*]quinoxaline	75 000	1500
MeIQ	2-amino-3-methylimidazo[4,5-*f*]quinoline	661 000	30 000
MeIQx	2-amino-3,4-dimethylimidazo[4,5-*f*]quinoxaline	145 000	14 000
4,8-DiMeIQx	2-amino-3,4,8-trimethylimidazo[4,5-*f*]quinoxaline	183 000	8000
PhIP	2-amino-1-methyl-6-phenylimidazo[4,5-*b*]pyridine	1800	120
AαC	2-amino-9*H*-pyrido[2,3-*b*]indole	300	20
MeAαC	2-amino-3-methyl-9*H*-pyrido[2,3-*b*]indole	200	120

Table 2. *In vivo* mutation spectra in small and large intestine for PhIP[20–25]

Animal	Target gene	No. mutants (%)						
		One-base substitution			One-base deletion		Other types of mutations	Total
		G:C to T:A	G:C to others	Others	G:C	Others		
Big Blue rat	*lacI**	56 (27)	57 (27)	7 (3)	72 (34)[§]	2 (1)	16 (8)	210 (100)
	*cII**	61 (42)	56 (39)	2 (1)	14 (10)	3 (2)	9 (6)	145 (100)
Big Blue mouse	*lacI**	56 (49)	21 (18)	4 (3)	30 (26)[¶]	0	5 (4)	115 (100)
Muta mouse	*lacZ*[†]	13 (33)	12 (30)	1 (3)	8 (20)	1 (3)	5 (13)	40 (100)
	cII[‡]	23 (70)	9 (27)	0	1 (3)	0	0	33 (100)
*gpt*Δ mouse	*gpt**	52 (53)	27 (27)	1 (1)	13 (13)	1 (1)	5 (5)	99 (100)
	*gam**	10 (11)	1 (1)	0	73 (83)	2 (2)	2 (2)	88 (100)

*Large intestine; [†]small and large intestine; [‡]small intestine; [§]includes 18 cases (8.5%) of GGGA to GGA mutation; [¶]includes eight cases (6.9%) of GGGA to GGA mutation.

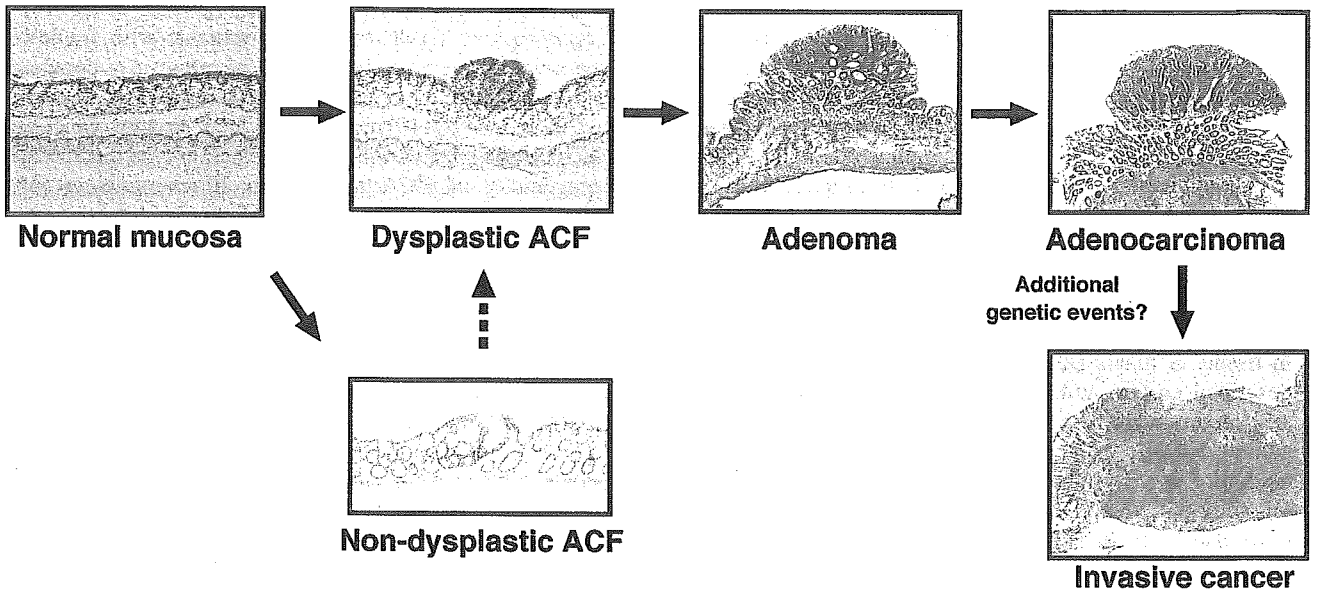

Fig. 2. Multi-stage model of rat colon cancer induced by PhIP. ACF, a candidate preneoplastic lesion of the colon, are induced shortly after exposure to PhIP. The majority of ACF are histologically non-dysplastic lesions with a subset of lesions demonstrating dysplastic features. Approximately one-quarter of dysplastic ACF harbor either *Apc* or β-*catenin* mutations. Dysplastic ACF may further progress into more dysplastic lesions, namely high-grade dysplastic ACF, adenomas and adenocarcinomas. The susceptibility gene, *Sct*, on rat chromosome 16 is considered to control the development of ACF.

Target organs of PhIP

The *in vivo* carcinogenic potential of PhIP against rodents has been extensively investigated. Using a standard long-term experimental protocol, it preferentially targets the colon and prostate in male rats, mammary glands in female rats, and lymphoid tissues in both male and female rats.[26] It is important to note that human cancers in the colon, mammary glands and prostate gland are common in Western countries, and are currently increasing in Japan where dietary habits are becoming more Westernized. Regarding the tissue-specific carcinogenicity of PhIP in rats, Lauber *et al.* recently reported that steroid hormone receptors, such as estrogen receptor α (ERα), estrogen receptor β (ERβ) and progesterone receptor (PR), are upregulated in PhIP-induced tumors. PhIP has estrogenic action, stimulates cell proliferation in an ER-dependent manner, and activates the mitogen-activated protein kinase (MAPK) signaling pathway through mRNA induction of *PR* and *c-myc* genes.[27] This could be a causative genetic event conferring tumors with the sex hormone dependency of PhIP-induced tumors. Compared with rats, the organ spectrum of PhIP in mice is more prevalent and restricted to lymphoid tissues.[9]

Colon carcinogenesis in rodents by PhIP

As described earlier, the colon is one of the most preferred target organs for cancer in rats induced by PhIP, especially in male rats. In contrast, mice rarely develop colon cancers after standard long-term PhIP-feeding protocols. We previously reported the development of small-intestinal cancers in C57BL/6 N mice, but not colon cancers, with a short-term PhIP-feeding protocol with a high-fat diet. Molecular mechanisms underlying the topographic difference between rats and mice in terms of site preference for tumor development remain to be elucidated.

When rats were fed PhIP at concentrations of 25–400 p.p.m. in their diet, they developed aberrant crypt foci (ACF), candidate neoplastic lesions in the colon, shortly after exposure to PhIP. A subset of ACF features dysplastic components in cryptic cells, and these dysplastic ACF often demonstrate β-catenin accumulation in either the cytoplasm or nucleus. Some of them harbor mutations in the β-*catenin* gene at codons responsible for the stability of the β-catenin protein. In particular, lesions harboring β-*catenin* mutations and demonstrating nuclear accumulation of β-catenin tend to demonstrate more dysplastic features. We have categorized these lesions as ACF with high-grade dysplasia ('high-grade dysplastic ACF'). Mutation spectra detected in dysplastic ACF, especially in high-grade dysplastic ones, are similar to those observed in colon cancers induced by PhIP, as detailed later. Furthermore, mucin detected by alcian blue-periodic acid Schiff (AB-PAS) staining is almost completely depleted in these high-grade dysplastic ACF.

As for the induction of colon cancers by long-term standard animal experiments, F344 male rats frequently develop colon carcinomas, the incidence being approximately 50% at 52 weeks when animals are fed continuously with a diet containing 400 p.p.m. PhIP.[26] With 100 p.p.m. PhIP in their diet, it takes approximately 2 years to get a ~50% cancer incidence in the colon, but no colon carcinomas were observed in 2 years with 25 p.p.m. PhIP.[28] This result tells us that there is a clear dose-dependency in the induction of cancers in the colon. Colon cancers induced by PhIP occur preferentially in the middle or distal part of the colon, and feature mostly polypoid growth. Most of the tumors are histologically

 doi: 10.1111/j.1349-7006.2005.00107.x

Table 3. Mutation spectra of β-*catenin* and *Apc* genes in colonic lesions induced by an intermittent PhIP-administration protocol in combination with a high fat diet[29,39]

Gene	Mutation spectrum			No. lesions with mutations*		
	Mutated position	Type of mutation	Amino acid change	Dysplastic ACF	High-grade dysplastic ACF	Colon cancer
β-*catenin*	Codon 32	GAT → AAT	Asp → Asn			2
		GAT → GGT	Asp → Gly	1		1†
	Codon 34	GGA → GTA	Gly → Val	4	1	2
		GGA → GAA	Gly → Glu			3†
	Codon 36	CAC → CCC	His → Pro			1‡
		CAC → TAC	His → Tyr		1	
	Codon 38	GGT → CGT	Gly → Arg			1‡
Apc	Codon 1413 in Exon 15	GGGA → GGA				1§
	Intron10/ exon11 boundary	tagGGGGG → tatGGGGG		1		1
	Total no. lesions analyzed			26	3	15

*Colonic lesions are histologically classified into dysplastic ACF, high-grade dysplastic ACF (microadenoma) and colon cancers, and the number of lesions with specific mutations observed in each type of lesions are indicated; †‡one case of colon cancer harbored mutations in both codons 32 and 34, and another one had them in both codons 36 and 38; §the same mutation was observed in colon cancers induced by long-term continuous feeding with PhIP.[37]

diagnosed as well-differentiated tubular adenocarcinomas, and the lesions rarely invade into submucosal layers or metastasize to other organs. Paneth cells are frequently observed in PhIP-induced colon cancers, as described later. Chronological multistep profiles for the development of colon cancers from normal colonic epithelial cells through ACF and dysplastic ACF deduced by sequential histological and genetic analyzes are shown in Figure 2.

Modulation of PhIP-induced colon carcinogenesis

It is interesting to note that induction of colon cancers by a short-term intermittent feeding protocol of 400 p.p.m. PhIP in combination with a high-fat diet was almost equivalent to that observed by a conventional long-term PhIP (400 p.p.m.)-feeding protocol.[29] That is, 10- to 20-fold less PhIP was enough for colon cancer induction when the former protocol was adopted compared with the latter conventional protocol[29] (H Nakagama *et al.*, unpublished observations). This indicates that experimental protocols themselves have a substantial effect on PhIP colon carcinogenesis. Furthermore, high-fat feeding accelerated the induction of colon carcinogenesis[30,31] as well as it did for mammary carcinogenesis induced by PhIP.[32] Diets high in calcium also showed a significant increase in the number of ACF and colon cancers compared with a low-calcium diet.[30] However, docosahexaenoic acid (DHA), a major component of fish oil, suppresses the formation of ACF and colon carcinomas after PhIP administration.[33]

Genetic alterations in PhIP-induced colonic lesions

Genetic analysis of PhIP-induced colon carcinomas has been carried out intensively by several groups, including ours.[34–36] Activation of the Wnt-β-catenin canonical signaling pathway is mainly caused by mutations in the β-*catenin* or *Apc* genes[34–39], similar to the process that occurs in human colon cancers.[40] Some of the lesions, however, do not have mutations in either of the genes.[29,39] Reduced expression of the Apc protein is also observed (H Nakagama *et al.*, unpublished observations). Mutations in the β-*catenin* gene are commonly observed, mainly at codons 32, 34, 36 or 38 in exon 2 (exon 3 in the human β-*catenin* gene), the majority of which are G to T or G to A base substitutions (Table 3). Mutations in the *Apc* gene are somehow characteristic of PhIP, as has been described previously;[37] one G deletion occurs at G-stretch sequences (5′-GGGA-3′ to 5′-GGA-3′) in exons 14 and 15, and a G to T transversion mutation in a G stretch (5′-tagGGGGG-3′ to 5′-tatGGGGG-3′) occurs at the boundary of intron 10 and exon 11. This type of mutation at G-stretches is in good agreement with those observed as characteristic *in vivo* mutation spectra using shuttle vector systems.[41] In contrast to colon cancers induced in humans and in mice and rats by azoxymethane, which is another colon carcinogen widely used for cancer induction in animal experiments, K-*ras* mutations are rarely observed in PhIP-induced colon cancers.[42] Induction of *p53* mutations is also a rare event in PhIP-induced colon cancers.[42,43]

Another interesting observation is that *Apc* mutation frequency was significantly decreased from approximately 50% (4 of 8)[37] to 13% (2 of 15) by feeding rats with a high-fat diet with PhIP,[29,39] indicating that the promoting effect of a high-fat diet does not simply enhance the growth of cell populations with *Apc* mutations, but may also alter the repertoire of genetic alterations required for the development of PhIP colon cancers under a high-fat feeding regime. This phenomenon is reminiscent of the effect of dietary fat on Ha-*ras* gene mutations at codons 12 and 13 in PhIP-induced rat mammary gland tumors.[44]

Table 4. Comparison of over- and underexpressed gene profiles in tumors of rats and humans[49–52]

Gene name	Rat (fold change)	Human
Overexpressed		
Defensin NP1 (α1)-like protein	53.3	Overexpressed†
Matrilysin (Mmp-7) mRNA	41.9	8.0-fold
(EST) AA859937	14.4	NA
Defensin NP3 (α3) gene	13.5	Overexpressed†
Platelet phospholipase A2	12.0	Overexpressed
Type I keratin (Mhr a-1)	9.9	NA
Anti-acetylcholine receptor antibody gene	9.6	NA
Mash-2 mRNA expressed in neuronal precursor cells	9.6	Overexpressed
c-Ha-ras proto-oncogene mechanism sequence	8.9	NA
Intracellular calcium-binding protein Mrp14	8.2	Overexpressed
Receptor-linked protein tyrosine phosphatase	8.1	NA
Macrophage metalloelastase (Mme)	7.5	5.1-fold
Cation transporter Oct1A	7.4	NA
VL30 element	6.8	NA
Interleukin 1-β mRNA	6.0	Unchanged
Cyclin D2	5.6	Overexpressed
α2-macroglobulin	5.6	Overexpressed
Underexpressed		
(EST) AA799832	40.4	NA
H36-α7 integrin α chain	15.6	2.8-fold
Neuron-specific protein Pep-19 mRNA, complete cds	13.6	2.1
Sc1 protein	12.2	4.5-fold
Zg-16p	11.4	NA
α, b-crystallin-related protein	11.3	NA
Dihydropyridine-sensitive L-type calcium channel	10.4	Unchanged
α-Crystallin B chain	10.2	4.3-fold
(EST) AF119148/Filamin C, gamma	9.6	5.8-fold
Alanine aminotransferase mRNA	9.4	NA
Insulin-like growth factor-binding protein	9.3	1.6-fold
(EST) AA892888/ RIKEN cDNA 0610006F02	7.8	NA
Carbonic anhydrase IV	7.7	2-fold
(EST) AA800735/Supervillin (predicted)	7.2	NA
Guanylin	6.0	20-fold
Phosphatase C-β1b	5.8	NA
Ssecks 322	5.7	NA
D-binding protein	5.1	Underexpressed

Data for human cancers was drawn from various database and literature sources.[49–52] †Although α1 and α3 defensins have not been reported to be overexpressed in human colon cancer, α5 defensin, which is another member of the Paneth cell-specific defensins, is overexpressed in both adenomas and adenocarcinomas of the colon in humans.[51] NA, data not available.

Genomic instability induced by PhIP

PhIP has been reported to induce various types of genomic instability. In PhIP-induced colon cancers, microsatellite alterations were observed in some cases.[45] PhIP also induces size alterations of minisatellite DNA sequences,[46] which are composed of much longer repetitive units than microsatellite DNA and are dispersed in the genome. Intriguingly, Bardelli *et al.* reported that exposure to specific carcinogens could select tumor cells with distinct forms of genomic instability, and human colon cancer cells, HCT116 and DLD1, which became resistant to PhIP in culture conditions, exhibited a chromosomal instability.[47] Because PhIP produces a bulky adduct, in contrast to the alkylation of guanine bases by alkylating agents such as *N*-methyl-*N*^{1}-nitro-*N*-nitrosoguanidine, PhIP-adducted DNA could result in the induction of chromosome breaks through nucleotide excision repair processes.[47] Later, Christian *et al.* demonstrated a cytogenetic signature of PhIP-induced mammary carcinomas using comparative genomic hybridization analysis,[48] but not in PhIP-induced colon cancers yet.

Gene expression profiles

Global gene expression analysis of PhIP-induced colon cancers using a high-density oligonucleotide microarray revealed that 27 and 46 of approximately 8800 genes or expressed sequence tags (EST) were over- and underexpressed, respectively, by threefold or greater in colon cancers.[49] For example, *defensins*, *matrylysin* (*MMP7*), *macrophage metalloelastase (Mme)* and *cyclin D2* are highly expressed. In contrast, genes encoding carbonic anhydrase IV, mucin-like proteins, and muscle-related proteins are underexpressed, similar to the situation in human colon cancers. *Insulin-like growth factor-binding*

 doi: 10.1111/j.1349-7006.2005.00107.x

protein gene (*IGF-BP*) and a gene related to *supervillin* were also markedly underexpressed.

A substantial number of genes in the list of over- and underexpressed genes in PhIP-induced colon cancers are either over- or underexpressed in human colon cancers as well (Table 4). For example, *defensin* family genes, $\alpha 5$ and $\alpha 6$, were previously reported to be upregulated in human colon cancers as noted in the SAGE database.[52] Furthermore, when six genes that are commonly overexpressed in PhIP colon cancers but have not been reported yet in human colon cancers, were analyzed by real-time reverse transcription–polymerase chain reaction (RT–PCR), four of them were demonstrated to be highly overexpressed in human colon cancers as well (H Nakagama *et al.*, unpublished observations). Taking all these available data together, a substantial similarity does exist between colon cancers of humans and those induced in rats by PhIP.

Aberrant differentiation of Paneth cells in colon cancer

We also found that a subset of genes whose expression is characteristic of Paneth cells, namely the *intestinal-type defensins* and *matrilysin*, were overexpressed in colon cancers. Hematoxylin and eosin and AB-PAS staining revealed the presence of Paneth granules in colon cancer cells, and lysozyme expression was also observed in cells with Paneth granules.[49] Although molecular mechanisms underlying Paneth cell differentiation in colon cancer tissues have not been fully elucidated yet, activation of the Wnt/Apc/β-catenin signaling pathway could be a causative event. In fact, van Es *et al.* has recently reported activation of Wnt signaling to induce maturation of Paneth cells in intestinal crypts.[53] The appearance of Paneth cells may reflect the aberrant differentiation of colonic stem cells in cancer tissues.

Preneoplastic lesions of the colon

As for preneoplastic lesions of the colon, several candidates have been proposed. ACF, which were first reported by Bird in 1987 as precancerous lesions of the colon,[54] β-catenin accumulated crypts (BCAC)[55] and MDF[56] have been identified. Recently, flat dysplastic ACF was proposed as a strong candidate for preneoplastic lesions of the colon.[57] In the case of the classical type of ACF by Bird,[54] which appears shortly after PhIP administration, most of the lesions are non-dysplastic, without any mutations in the β-*catenin* or *Apc* genes.[39] A group of ACF harbor dysplastic components in cryptic cells, and are categorized as dysplastic ACF. A small fraction of dysplastic ACF that feature high-grade dysplasia lack mucin production in cells detected by AB-PAS staining. Lesional identities among high-grade dysplastic ACF, MDF, BCAC and flat dysplastic ACF are still a point of great and long dispute, but all of these lesions demonstrate β-*catenin* mutations and/or intense accumulation of β-catenin protein, and a drastic decrease in or depletion of mucin. Again, an appearance of Paneth cells is also occasionally observed in these dysplastic lesions, similar to the situation in colon cancers, as described earlier.[39]

Differential staining for dysplastic lesions in the colon

We have recently developed a novel and simple method to identify dysplastic ACF. By adding the step of a decolorization process with 70% methanol after conventional 0.2% methylene-blue staining, dysplastic ACF were easily and differentially contrasted as depicted in Figure 3A ('Ochiai-Nakagama method').[58] Furthermore, some of the dysplastic lesions became evident only after this differential staining procedure and, furthermore, the number of dysplastic ACF detected by this novel method more precisely reflected the carcinogenic potential of PhIP than the total number of ACF.[58] Examples are depicted in Figure 3Ba–f. Some of the lesions demonstrate heterogeneous features (Fig. 3Ba,b). The presence of this kind of lesion may suggest that the sequential transition from non-dysplastic to dysplastic ACF and also from dysplastic to high-grade dysplastic lesions within a lesion may occur in a subset of ACF. Lesions in Figures 3Bc–f demonstrate the typical features of high-grade dyplastic ACF. Both lesions characteristically demonstrated aberrant crypts with small or pin-holed orifices of crypts, and irregular alignments of crypts in the lesion. As for the lesion represented in Figure 3e, the lesion is very tiny when observed from the surface; however, histological examination revealed the actual size of this lesion to be much larger: it was embedded in the mucosal layer, with dysplastic components along with Paneth cells.

Differential susceptibility to colon carcinogenesis

Differential susceptibility to the development of colon cancers induced by PhIP is observed between male and female F344 rats,[25] although DNA-adduct levels and *in vivo* mutation frequencies measured using the *lacI* shuttle vector system are almost equivalent.[59] Ochiai *et al.* found that levels of cell proliferation in colon epithelial cells measured by BrdU incorporation after PhIP exposure were approximately 1.5-fold higher in male than in female rats, and this may confer a sexual difference.[59]

Strain differences in the susceptibility to PhIP colon carcinogenesis are also observed. The average number of ACF induced by PhIP varies widely among rat strains. BUF rats are highly sensitive, F344 and Brown-Norway are moderately sensitive, and ACI are resistant in terms of the induction of ACF.[60] F344 rats are indeed more susceptible to the induction of colon cancers compared with the ACI strain. Genetic traits responsible for differential susceptibility to the development of ACF by PhIP (we named this trait *Sct* [*susceptibility to colon tumor*]) were mapped on rat chromosome 16, between D16Rat17 and D16Wox3,[35] and research toward identification of the responsible gene(s) is currently being conducted intensively in our laboratory.

Epidemiological studies for human risk from PhIP

High-temperature cooking techniques and the 'doneness' level of red meat have been linked to the development of

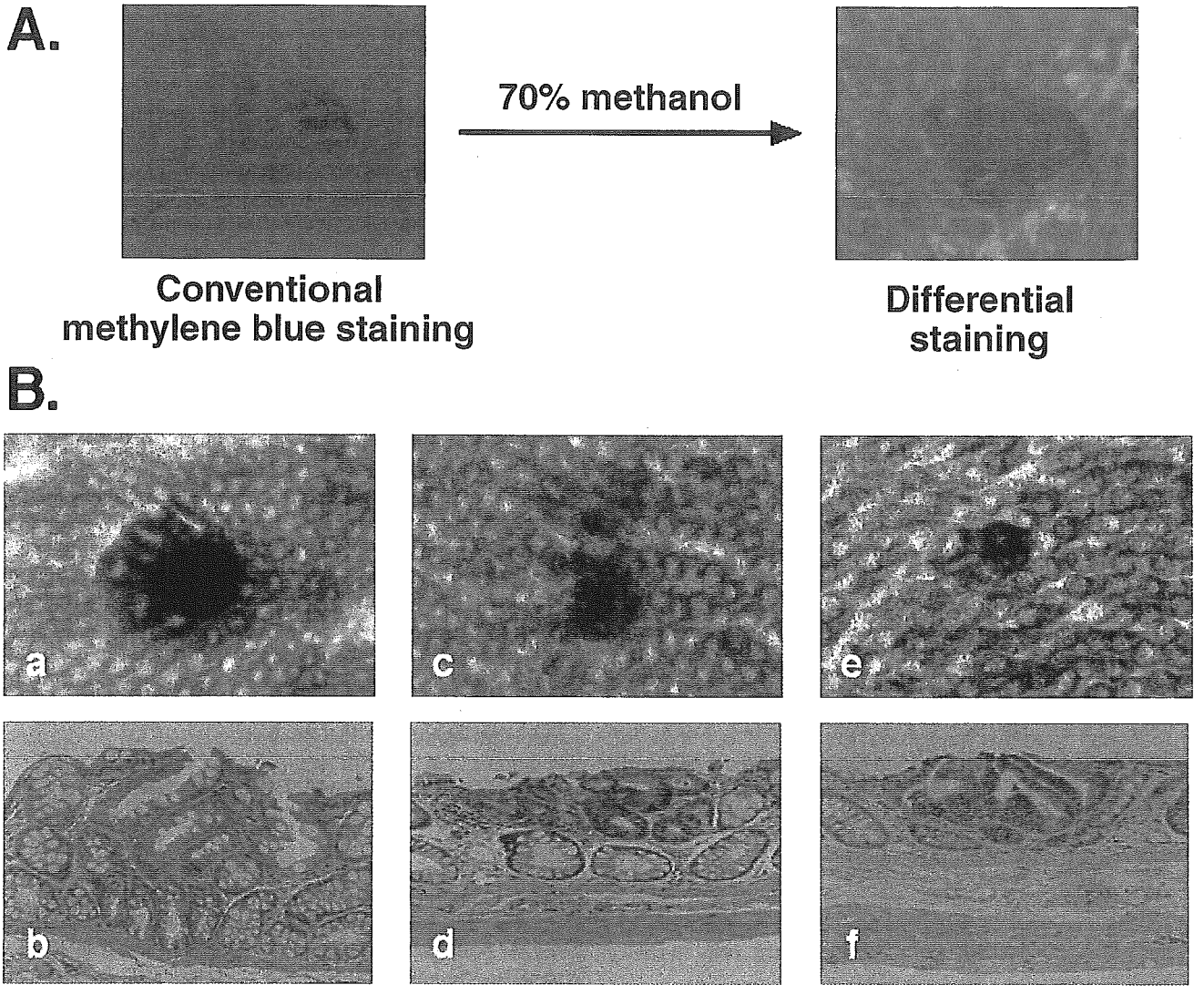

Fig. 3. Differential staining, a simple and efficient method for selectively contrasting dysplastic lesions in the colon induced by PhIP. (A) For conventional methylene blue staining of ACF, strips of colon tissues are fixed in 10% neutralized formalin overnight at 4°C, and stained with 0.2% methylene blue in phosphate-buffered saline for 30 min. For differential staining, tissues strips are subsequently decolorized with 70% methanol with gentle shaking at room temperature for 4–6 min. Dysplastic ACF detected after the differential staining are characterized as lesions containing crypt(s) with homogeneously dense staining, and relatively small or even undetectable orifices of the crypts compared with normal crypts. Non-dysplastic ACF, in contrast, are composed of crypts with clear orifices and are stained relatively lightly compared to dysplastic ones. Some of the non-dysplastic lesions even became undetectable after the decolorization process. (B) Representative features of dysplastic ACF. (a,c,e) Digitized images of lesions detected by differential staining and (b,d,f) their respective histological features on hematoxylin and eosin staining are presented. Some dysplastic lesions (c,e), which show high-grade dysplasia (d,f), became evident only after the differential staining.

colorectal cancer, and Sinha and colleagues found that an elevated risk of colorectal adenomas is mainly due to an association with well-done/very well-done red meat consumption using an HCA database linked to a questionnaire to estimate HCA consumption.[61,62] Well-done meat has also been reported to be associated with increased risks of mammary and prostate gland carcinomas in humans.[9,63] Recently, Chao *et al.* further extended their study and reported that prolonged high levels of consumption of processed meat was associated with an increase in the risk of distal colon cancer after adjusting for age and energy intake.[64] Long-term consumption of poultry and fish was inversely associated with risk of both proximal and distal colon cancer, and high levels of consumption of red meat was associated with a higher risk of rectal cancer.[64] When considering human risk from PhIP, the effects of transplacental exposure to PhIP[65] and of PhIP-exposure in newborn babies on the generation of human cancers[66] should also be carefully investigated. In addition, the possible existence of a practical threshold value for the induction of cancers by PhIP[67] should be taken into consideration for assessment of its risk to humans, and further investigation is warranted in the future to clarify this point. It is practically important to note that because PhIP is the most abundant colon carcinogenic HCA in cooked meat and fish, to lessen the total amount of HCA intake from diet by, for example, avoiding high levels of consumption of red

 doi: 10.1111/j.1349-7006.2005.00107.x

and processed meat and using a microwave oven or flipping meat during cooking, are recommended to decrease the chance of colon cancer development to some extent.

Future prospective views of the PhIP-induced colon cancer model

As is widely recognized, human cancers are caused by the combined effects of both hereditary and environmental factors. As for environmental factors, HCA are some of the most abundant genotoxic mutagens in our environment, and humans are exposed to them in their day-to-day lives. This has been evidenced by the presence of PhIP and PhIP-DNA adducts in human tissues. We therefore strongly believe that PhIP-induced colon cancer models in rats could serve as a powerful and relevant model system for the investigation of human colon carcinogenesis. Furthermore, numerous other compounds that can modulate the process of PhIP colon carcinogenesis, such as fat, inflammatory agents and other mutagenic/carcinogenic compounds, also exist abundantly in our environment. Although we do not have sufficient data on the combined effects of these environmental compounds on human carcinogenesis, synergistic effects from, for example, a mixture of various HCA and other non-genotoxic modulating compounds could reasonably be expected. This hypothesis could easily be recapitulated and evaluated in this rat model system. In fact, we have recently found that a combination of PhIP with some alkylating agents produced poorly differentiated and invasive adenocarcinomas in the rat colon. More detailed and comprehensive analysis should be conducted to assess the overall risk to humans from PhIP and also from other HCA in terms of its impact on human carcinogenesis. Moreover, Tanaka *et al.* have recently succeeded in inducing colon cancers using PhIP in mice in the presence of dextran sodium sulfate-induced colonic inflammation.[36] This mouse model is also of great benefit, and further extends the possibility and usefulness of PhIP-induced colon cancer models in rodents for the investigation of the molecular mechanisms of colon carcinogenesis, including those related to inflammation-related cancer development and those responsible for the genetic susceptibility of individual animals.

Acknowledgments

The authors are grateful to Drs Takashi Sugimura, Minako Nagao and Hiroshi Tazawa for critical reading of this article, and would also like to thank Kyoko Fujiwara, Ayako Taguchi and Ryoichi Masui for their continuing contribution to the work performed in our laboratory. This study was supported in part by Grants-in-Aid for Cancer Research and for the 2nd and 3rd Term of the Comprehensive 10-Year Strategy for Cancer Control from the Ministry of Health, Labour and Welfare of Japan, and by a Grant-in-Aid for Scientific Research on Priority Area (C) from the Ministry of Education, Culture, Sports, Science and Technology of Japan. MN was the recipient of a Research Resident Fellowship from the Foundation for Promotion of Cancer Research in Japan.

References

1 Lichtenstein P, Holm NV, Verkasalo PK *et al.* Environmental and heritable factors in the causation of cancer: analyses of cohorts of twins from Sweden, Denmark, and Finland. *N Engl J Med* 2000; **343**: 78–85.
2 Doll R, Peto R. The causes of cancer: quantitative estimates of avoidable risks of cancer in the United States today. *J Natl Cancer Inst* 1981; **66**: 1191–308.
3 Coussens LM, Werb Z. Inflammation and cancer. *Nature* 2002; **420**: 860–7.
4 Houessou JK, Benac C, Delteil C, Camel V. Determination of polycyclic aromatic hydrocarbons in coffee brew using solid-phase extraction. *J Agric Food Chem* 2005; **53**: 871–9.
5 Sugimura T, Nagao M, Wakabayashi K. How we should deal with unavoidable exposure of man to environmental mutagens: cooked food mutagen discovery, facts and lessons for cancer prevention. *Mutat Res* 2000; **447**: 15–25.
6 Sugimura T. Nutrition and dietary carcinogens. *Carcinogenesis* 2000; **21**: 387–95.
7 Felton JS, Knize MG, Shen NH *et al.* The isolation and identification of a new mutagen from fried ground beef: 2-amino-1-methyl-6-phenylimidazo[4,5-*b*]pyridine (PhIP). *Carcinogenesis* 1986; **7**: 1081–6.
8 Nagao M, Honda M, Seino Y, Yahagi T, Sugimura T. Mutagenicities of smoke condensates and the charred surface of fish and meat. *Cancer Lett* 1977; **2**: 221–6.
9 Sugimura T, Wakabayashi K, Nakagama H, Nagao M. Heterocyclic amines: Mutagens/carcinogens produced during cooking of meat and fish. *Cancer Sci* 2004; **95**: 290–9.
10 Schut HA, Snyderwine EG. DNA adducts of heterocyclic amine food mutagens: implications for mutagenesis and carcinogenesis. *Carcinogenesis* 1999; **20**: 353–68.
11 Felton JS, Knize MG, Salmon CP, Malfatti MA, Kulp KS. Human exposure to heterocyclic amine food mutagens/carcinogens: relevance to breast cancer. *Environ Mol Mutagen* 2002; **39**: 112–8.
12 Augustsson K, Skog K, Jagerstad M, Steineck G. Assessment of the human exposure to heterocyclic amines. *Carcinogenesis* 1997; **18**: 1931–5.
13 Hashimoto H, Hanaoka T, Kobayashi M, Tsugane S. Analytical method of 2-amino-1-methyl-6-phenylimidazo[4,5-*b*]pyridine in human hair by column-switching liquid chromatography-mass spectrometry. *J Chromatogr B Analyt Technol Biomed Life Sci* 2004; **803**: 209–13.
14 Takayama K, Yamashita K, Wakabayashi K, Sugimura T, Nagao M. DNA modification by 2-amino-1-methyl-6-phenylimidazo[4,5-*b*]pyridine in rats. *Jpn J Cancer Res* 1989; **80**: 1145–8.
15 Lin D, Kaderlik KR, Turesky RJ, Miller DW, Lay JO Jr, Kadlubar FF. Identification of N-(Deoxyguanosin-8-yl)-2-amino-1-methyl-6-phenylimidazo [4,5-*b*]pyridine as the major adduct formed by the food-borne carcinogen, 2-amino-1-methyl-6-phenylimidazo[4,5-*b*]pyridine, with DNA. *Chem Res Toxicol* 1992; **5**: 691–7.
16 Shirai T, Takahashi S, Cui L *et al.* Use of polyclonal antibodies against carcinogen-DNA adducts in analysis of carcinogenesis. *Toxicol Lett* 1998; **102–103**: 441–6.
17 Friesen MD, Kaderlik K, Lin D *et al.* Analysis of DNA adducts of 2-amino-1-methyl-6-phenylimidazo[4,5-*b*]pyridine in rat and human tissues by alkaline hydrolysis and gas chromatography/electron capture mass spectrometry: validation by comparison with ^{32}P-postlabeling. *Chem Res Toxicol* 1994; **7**: 733–9.
18 Dingley KH, Curtis KD, Nowell S, Felton JS, Lang NP, Turteltaub KW. DNA and protein adduct formation in the colon and blood of humans after exposure to a dietary-relevant dose of 2-amino-1-methyl-6-phenylimidazo-[4,5-*b*]pyridine. *Cancer Epidemiol Biomarkers Prev* 1999; **8**: 507–12.
19 Yadollahi-Farsani M, Gooderham NJ, Davies DS, Boobis AR. Mutational spectra of the dietary carcinogen 2-amino-1-methyl-6-phenylimidazo[4,5-*b*]- pyridine (PhIP) at the Chinese hamsters *hprt* locus. *Carcinogenesis* 1996; **17**: 617–24.
20 Okonogi H, Stuart GR, Okochi E *et al.* Effects of gender and species on spectra of mutation induced by 2-amino-1-methyl-6-phenylimidazo[4,5-*b*]pyridine in the lacI transgene. *Mutat Res* 1997; **395**: 93–9.
21 Stuart GR, Thorleifson E, Okochi E *et al.* Interpretation of mutational spectra from different genes: analyses of PhIP-induced mutational specificity in the *lacI* and *cII* transgenes from colon of Big Blue rats. *Mutat Res* 2000; **452**: 101–21.
22 Okonogi H, Ushijima T, Zhang XB *et al.* Agreement of mutational characteristics of heterocyclic amines in *lacI* of the Big Blue mouse with those in tumor related genes in rodents. *Carcinogenesis* 1997; **18**: 745–8.
23 Masumura K, Matsui K, Yamada M *et al.* Characterization of mutations induced by 2-amino-1-methyl-6-phenylimidazo[4,5-*b*]pyridine in the

colon of *gpt* delta transgenic mouse: novel G:C deletions beside runs of identical bases. *Carcinogenesis* 2000; **21**: 2049–56.
24 Lynch AM, Gooderham NJ, Davies DS, Boobis AR. Genetic analysis of PHIP intestinal mutations in MutaMouse. *Mutagenesis* 1998; **13**: 601–5.
25 Itoh T, Kuwahara T, Suzuki T, Hayashi M, Ohnishi Y. Regional mutagenicity of heterocyclic amines in the intestine: mutation analysis of the *cII* gene in *lambda/lacZ* transgenic mice. *Mutat Res* 2003; **539**: 99–108.
26 Ito N, Hasegawa R, Sano M *et al.* A new colon and mammary carcinogen in cooked food, 2-amino-1-methyl-6-phenylimidazo[4,5-*b*]pyridine (PhIP). *Carcinogenesis* 1991; **12**: 1503–6.
27 Lauber SN, Ali S, Gooderham NJ. The cooked food derived carcinogen 2-amino-1-methyl-6-phenylimidazo[4,5-*b*] pyridine is a potent oestrogen: a mechanistic basis for its tissue-specific carcinogenicity. *Carcinogenesis* 2004; **25**: 2509–17.
28 Hasegawa R, Sano M, Tamano S *et al.* Dose-dependence of 2-amino-1-methyl-6-phenylimidazo[4,5-*b*]- pyridine (PhIP) carcinogenicity in rats. *Carcinogenesis* 1993; **14**: 2553–7.
29 Ubagai T, Ochiai M, Kawamori T *et al.* Efficient induction of rat large intestinal tumors with a new spectrum of mutations by intermittent administration of 2-amino-1-methyl-6- phenylimidazo[4,5-*b*]pyridine in combination with a high fat diet. *Carcinogenesis* 2002; **23**: 197–200.
30 Weisburger JH, Braley J, Reinhardt J *et al.* The role of fat and calcium in the production of foci of aberrant crypts in the colon of rats fed 2-amino-1-methyl- 6-phenylimidazo[4,5-*b*]pyridine. *Environ Health Perspect* 1994; **102** (Suppl. 6): 53–5.
31 Ochiai M, Nakagama H, Watanabe M, Ishiguro Y, Sugimura T, Nagao M. Efficient method for rapid induction of aberrant crypt foci in rats with 2-amino-1-methyl-6-phenylimidazo[4,5-*b*]pyridine. *Jpn J Cancer Res* 1996; **87**: 1029–33.
32 Ghoshal A, Preisegger KH, Takayama S, Thorgeirsson SS, Snyderwine EG. Induction of mammary tumors in female Sprague-Dawley rats by the food-derived carcinogen 2-amino-1-methyl-6-phenylimidazo[4,5-*b*]pyridine and effect of dietary fat. *Carcinogenesis* 1994; **15**: 2429–33.
33 Takahashi M, Totsuka Y, Masuda M *et al.* Reduction in formation of 2-amino-1-methyl-6-phenyl- imidazo[4,5-*b*]pyridine (PhIP)-induced aberrant crypt foci in the rat colon by docosahexaenoic acid (DHA). *Carcinogenesis* 1997; **18**: 1937–41.
34 Tsukamoto T, Tanaka H, Fukami H *et al.* More frequent *beta-catenin* gene mutations in adenomas than in aberrant crypt foci or adenocarcinomas in the large intestines of 2-amino-1-methyl-6-phenylimidazo[4,5-*b*]pyridine (PhIP)-treated rats. *Jpn J Cancer Res* 2000; **91**: 792–6.
35 Nakagama H, Ochiai M, Ubagai T *et al.* A rat colon cancer model induced by 2-amino-1-methyl-6-phenyl- imidazo[4,5-*b*]pyridine, PhIP. *Mutat Res* 2002; **506–507**: 137–44.
36 Tanaka T, Suzuki R, Kohno H, Sugie S, Takahashi M, Wakabayashi K. Colonic adenocarcinomas rapidly induced by the combined treatment with 2-amino-1-methyl-6-phenylimidazo[4,5-*b*]pyridine and dextran sodium sulfate in male ICR mice possess *beta-catenin* gene mutations and increases immunoreactivity for beta-catenin, cyclooxygenase-2 and inducible nitric oxide synthase. *Carcinogenesis* 2005; **26**: 229–38.
37 Kakiuchi H, Watanabe M, Ushijima T *et al.* Specific 5′-GGGA-3′ – >5′-GGA-3′ mutation of the *Apc* gene in rat colon tumors induced by 2-amino-1-methyl-6-phenylimidazo- [4,5-*b*]pyridine. *Proc Natl Acad Sci USA* 1995; **92**: 910–4.
38 Dashwood RH, Suzui M, Nakagama H, Sugimura T, Nagao M. High frequency of *beta-catenin* (*ctnnb1*) mutations in the colon tumors induced by two heterocyclic amines in the F344 rat. *Cancer Res* 1998; **58**: 1127–9.
39 Ochiai M, Ushigome M, Fujiwara K *et al.* Characterization of dysplastic aberrant crypt foci in the rat colon induced by 2-amino-1-methyl-6-phenylimidazo[4,5-*b*]pyridine. *Am J Pathol* 2003; **163**: 1607–14.
40 Morin PJ, Sparks AB, Korinek V *et al.* Activation of β-catenin-Tcf signaling in colon cancer by mutations in β-*catenin* or *APC*. *Science* 1997; **275**: 1787–90.
41 Nagao M. A new approach to risk estimation of food-borne carcinogens – heterocyclic amines – based on molecular information. *Mutat Res* 1999; **431**: 3–12.
42 Toyota M, Ushijima T, Kakiuchi H *et al.* Genetic alterations in rat colon tumors induced by heterocyclic amines. *Cancer* 1996; **77**: 1593–7.
43 Makino H, Ushijima T, Kakiuchi H *et al.* Absence of *p53* mutations in rat colon tumors induced by 2-amino-6-methyldipyrido[1,2-a: 3′,2′-d]imidazole, 2-amino-3-methylimidazo[4,5-*f*]quinoline, or 2-amino-1-methyl-6-phenyl-imidazo[4,5-*b*]pyridine. *Jpn J Cancer Res* 1994; **85**: 510–4.
44 Roberts-Thomson SJ, Snyderwine EG. Effect of dietary fat on codon 12 and 13 Ha-*ras* gene mutations in 2-amino-1-methyl-6-phenylimidazo[4,5-*b*]- pyridine-induced rat mammary gland tumors. *Mol Carcinog* 1997; **20**: 348–54.
45 Nagao M, Ushijima T, Toyota M, Inoue R, Sugimura T. Genetic changes induced by heterocyclic amines. *Mutat Res* 1997; **376**: 161–7.
46 Kitazawa T, Kominami R, Tanaka R, Wakabayashi K, Nagao M. 2-Hydroxyamino-1-methyl-6-phenylimidazo[4,5-*b*]pyridine induction of recombinational mutations in mammalian cell lines as detected by DNA fingerprinting. *Mol Carcinog* 1994; **9**: 67–70.
47 Bardelli A, Cahill DP, Lederer G *et al.* Carcinogen-specific induction of genetic instability. *Proc Natl Acad Sci USA* 2001; **98**: 5770–5.
48 Christian AT, Snyderwine EG, Tucker JD. Comparative genomic hybridization analysis of PhIP-induced mammary carcinomas in rats reveals a cytogenetic signature. *Mutat Res* 2002; **506–507**: 113–9.
49 Fujiwara K, Ochiai M, Ohta T *et al.* Global gene expression analysis of rat colon cancers induced by a food-borne carcinogen, 2-amino-1-methyl-6-phenylimidazo[4,5-*b*]pyridine. *Carcinogenesis* 2004; **25**: 1495–505.
50 Notterman DA, Alon U, Sierk AJ, Levine AJ. Transcriptional gene expression profiles of colorectal adenoma, adenocarcinoma, and normal tissue examined by oligonucleotide arrays. *Cancer Res* 2001; **61**: 3124–30.
51 Buckhaults P, Rago C, St Croix B *et al.* Secreted and cell surface genes expressed in benign and malignant colorectal tumors. *Cancer Res* 2001; **61**: 6996–7001.
52 National Institutes of Health. SAGE [Internet document]. Available from URL: http://ncbi.nim.nih.gov/projects/geo/gds/gds_browse.cgi?gds=550
53 van Es JH, Jay P, Gregorieff A *et al.* Wnt signalling induces maturation of Paneth cells in intestinal crypts. *Nat Cell Biol* 2005; **7**: 381–6.
54 Bird RP. Observation and quantification of aberrant crypts in the murine colon treated with a colon carcinogen: preliminary findings. *Cancer Lett* 1987; **37**: 147–51.
55 Yamada Y, Yoshimi N, Hirose Y *et al.* Sequential analysis of morphological and biological properties of beta-catenin-accumulated crypts, provable premalignant lesions independent of aberrant crypt foci in rat colon carcinogenesis. *Cancer Res* 2001; **61**: 1874–8.
56 Caderni G, Femia AP, Giannini A *et al.* Identification of mucin-depleted foci in the unsectioned colon of azoxymethane-treated rats: correlation with carcinogenesis. *Cancer Res* 2003; **63**: 2388–92.
57 Paulsen JE, Loberg EM, Olstorn HB, Knutsen H, Steffensen IL, Alexander J. Flat dysplastic aberrant crypt foci are related to tumorigenesis in the colon of azoxymethane-treated rat. *Cancer Res* 2005; **65**: 121–9.
58 Ochiai M, Watanabe M, Nakanishi M, Taguchi A, Sugimura T, Nakagama H. Differential staining of dysplastic aberrant crypt foci in the colon facilitates prediction of carcinogenic potentials of chemicals in rats. *Cancer Lett* 2005; **220**: 67–74.
59 Ochiai M, Watanabe M, Kushida H, Wakabayashi K, Sugimura T, Nagao M. DNA adduct formation, cell proliferation and aberrant crypt focus formation induced by PhIP in male and female rat colon with relevance to carcinogenesis. *Carcinogenesis* 1996; **17**: 95–8.
60 Ishiguro Y, Ochiai M, Sugimura T, Nagao M, Nakagama H. Strain differences of rats in the susceptibility to aberrant crypt foci formation by 2-amino-1-methyl-6-phenylimidazo[4,5-*b*]pyridine: no implication of *Apc* and *Pla2g2a* genetic polymorphisms in differential susceptibility. *Carcinogenesis* 1999; **20**: 1063–8.
61 Sinha R, Chow WH, Kulldorff M *et al.* Well-done, grilled red meat increases the risk of colorectal adenomas. *Cancer Res* 1999; **59**: 4320–4.
62 Sinha R, Rothman N. Role of well-done, grilled red meat, heterocyclic amines (HCAs) in etiology of human cancer. *Cancer Lett* 1999; **143**: 189–94.
63 Norrish AE, Ferguson LR, Knize MG, Felton JS, Sharpe SJ, Jackson RT. Heterocyclic amine content of cooked meat and risk of prostate cancer. *J Natl Cancer Inst* 1999; **91**: 2038–44.
64 Chao A, Thun MJ, Connell CJ *et al.* Meat consumption and risk of colorectal cancer. *JAMA* 2005; **293**: 172–82.
65 Hasegawa R, Kimura J, Yaono M *et al.* Increased risk of mammary carcinoma development following transplacental and trans-breast milk exposure to a food-derived carcinogen, 2-amino-1-methyl-6-phenylimidazo[4,5-*b*]pyridine (PhIP), in Sprague-Dawley rats. *Cancer Res* 1995; **55**: 4333–8.
66 Miyauchi M, Nishikawa A, Furukawa F *et al.* Carcinogenic risk assessment of MeIQx and PhIP in a newborn mouse two-stage tumorigenesis assay. *Cancer Lett* 1999; **142**: 75–81.
67 Fukushima S, Wanibuchi H, Morimura K *et al.* Existence of a threshold for induction of aberrant crypt foci in the rat colon with low doses of 2-amino-1-methyl-6-phenylimidazo[4,5-*b*]pyridine. *Tox Sci* 2004; **80**: 109–14.

 doi: 10.1111/j.1349-7006.2005.00107.x

Unfolding of higher DNA structures formed by the d(CGG) triplet repeat by UP1 protein

Hirokazu Fukuda[1], Masato Katahira[2,3], Etsuko Tanaka[1], Yoshiaki Enokizono[2], Naoto Tsuchiya[1], Kumiko Higuchi[1], Minako Nagao[1] and Hitoshi Nakagama[1,*]

[1]*Biochemistry Division, National Cancer Center Research Institute, 1-1, Tsukiji 5, Chuo-ku, Tokyo 104-0045, Japan*
[2]*Department of Environment and Natural Sciences, Graduate School of Environment and Information Sciences, Yokohama National University, 79-7 Tokiwadai, Hodogaya-ku, Yokohama 240-8501, Japan*
[3]*Division of Molecular Biophysics, Science of Biological Supramolecular Systems, Yokohama City University, 1-7-29 Suehiro, Tsurumi-ku, Yokohama 230-0045, Japan*

Fragile X syndrome is caused by expansion of a d(CGG) triplet repeat in the 5′-untranslated region of the first exon of the *FMR1* gene resulting in silencing of the gene. The d(CGG) repeat has been reported to form hairpin and quadruplex structures *in vitro*, and formation of these higher structures could be responsible for its unstable expansion in the syndrome, although molecular mechanisms underlying the repeat expansion still remain elusive. We have previously proved that UP1, a proteolytic product of hnRNP A1, unfolds the intramolecular quadruplex structures of $d(GGCAG)_5$ and $d(TTAGGG)_4$ and abrogates the arrest of DNA synthesis at $d(GGG)_n$ sites. Here, we demonstrate that the d(CGG) repeat forms a peculiar DNA structure, which deviates from the canonical B-form structure. In addition, UP1 was demonstrated by CD spectrum analysis to unfold this characteristic higher structure of the d(CGG) repeat and to abrogate the arrest of DNA synthesis at the site. This ability of UP1 suggests that unfolding of unusual DNA structures of a triplet repeat is required for DNA synthesis processes.

Introduction

Fragile X syndrome is the most common form of inherited mental retardation in humans, and is caused by the silencing of the *FMR1* gene (for reviews, see Rousseau *et al.* 1992; Mandel 1993; Crawford *et al.* 2001). Transcriptional silencing of the *FMR1* gene results from expansion of a d(CGG) trinucleotide repeat in the 5′-untranslated region of the first exon of the gene and following hypermethylation in the repeat and promoter region. Allelic forms of the *FMR1* gene are classified by the number of CGG repeats into three groups: normal alleles are less than 50, premutation alleles range between 50 and 200, and fully affected alleles carry 200–2000 repeats. The $d(CGG)_n$ tract was reported to form hairpin (Chen *et al.* 1995; Gacy *et al.* 1995; Nadel *et al.* 1995; Fojtík *et al.* 2004), quadruplex (Fry & Loeb 1994; Kettani *et al.* 1995; Usdin & Woodford 1995), and homoduplex (Fojtík *et al.* 2004) structures *in vitro* under physiologic-like conditions. These higher structures of $d(CGG)_n$ were reported to cause the arrest of DNA synthesis in the repeat both *in vitro* and *in vivo* (Kang *et al.* 1995; Usdin & Woodford 1995; Samadashwily *et al.* 1997; Kamath-Loeb *et al.* 2001).

It is supposed that there are some mechanisms that unfold these unusual higher structures of the triplet repeat. However, molecular details underlying stable maintenance of the repeat are largely unknown. Several proteins have been reported to unfold or destabilize the higher structures of $d(CGG)_n$. WRN helicase unwinds these structures and abrogates the arrest of DNA synthesis at the site (Fry & Loeb 1999; Kamath-Loeb *et al.* 2001). Two quadruplex telomeric DNA binding proteins purified from rat liver, qTBP42 and uqTBP25, destabilize the quadruplex forms of the repeat (Weisman-Shomer *et al.* 2000). We previously identified UP1, a proteolytic product of hnRNP A1, as a $d(GGCAG)_n$ binding protein, and demonstrated UP1 to unfold the intramolecular quadruplex structure of $d(GGCAG)_5$ and $d(TTAGGG)_4$ (Fukuda *et al.* 2001, 2002). In the present report, we document that UP1 unfolds higher structures

Communicated by: Fuyuki Ishikawa
**Correspondence*: E-mail: hnakagam@gan2.res.ncc.go.jp

DOI: 10.1111/j.1365-2443.2005.00896.x

of d(CGG)$_n$ and abrogates the arrest of DNA synthesis at the repeat.

Results

CD spectra of d(CGG)$_n$

According to previous reports, the d(CGG)$_n$ sequences form unusual DNA structures, hairpins, and quadruplexes under physiologic-like conditions (Fry & Loeb 1994; Chen *et al.* 1995; Gacy *et al.* 1995; Kettani *et al.* 1995; Nadel *et al.* 1995; Usdin & Woodford 1995; Fojtík *et al.* 2004). Whether the structure of the d(CGG) repeats could form either hairpins or quadruplexes seems to depend on the experimental conditions, including repeat sizes and coexistence of metal ions. We carried out CD spectrum analysis of the oligonucleotides CGG7 and CGG16 (see Experimental procedures) in the presence or absence of 150 mM KCl at 25 °C.

The CD spectrum of CGG7 showed a positive peak at 280 nm and a negative peak at 255 nm with comparable intensity in the absence of KCl, and this CD spectrum is characteristic of the canonical B-form structure (Fig. 1A). In the presence of 150 mM KCl, the CD spectrum of CGG7 showed a decrease of the positive peak at 280 nm and an increase of the negative peak at 255 nm (Fig. 1B). The pattern differed from the typical CD spectrum of the B-form structure, and suggested a structural conversion of the oligonucleotide from a B to a non-B structure. The CD spectrum of CGG7 at 150 mM KCl was obviously different from those of the quadruplexes with guanine quartets, the parallel stranded quadruplex (positive maxima at 260 and 210 nm), and the antiparallel stranded quadruplex (positive maxima at 295 and 210 nm, or at 295, 260, and 210 nm) (Dapic *et al.* 2003).

The CD spectrum of the oligonucleotide CGG16 in either the presence or absence of 150 mM KCl showed a characteristic pattern similar to that of CGG7 under 150 mM KCl conditions, in the sense that the negative peak at 255 nm is large while the positive peak at 280 nm is small (Fig. 1C,D). This suggests that the oligonucleotide CGG16 can mainly form a non-B structure regardless of the presence of K^+ ions. The CD spectrum of oligonucleotide CGG16mut, having C to A substitutions at two sites in CGG16 (see Experimental procedures), represented a typical pattern of the B structure with comparable negative and positive peaks at 255 nm and 280 nm, respectively, both in the presence and absence of 150 mM KCl (Fig. 1E,F), indicating that destruction of the continuation of d(CGG) repeats caused by C to A mutation strongly inhibits the formation of the non-B structure.

Effects of UP1 protein on DNA structures of d(CGG) repeats

Because UP1 was previously demonstrated to unfold the intramolecular quadruplex structure of d(GGCAG)$_5$ and d(TTAGGG)$_4$ (Fukuda *et al.* 2002; Myers *et al.* 2003), we investigated the effect of UP1 on secondary structures of the oligonucleotides, CGG7, CGG16, and CGG16mut, by CD analysis. In the presence of 150 mM KCl, in either CGG7 or CGG16, no drastic change in CD bands was observed on addition of GST-UP1 protein (Fig. 2B,D), the positive peak at 280 nm still being rather small. This indicates that UP1 does not have a sufficient effect on the non-B form of d(CGG) repeats under 150 mM KCl conditions. In the absence of KCl, the positive peak of CGG16 at 280 nm was increased by addition of GST-UP1 in a concentration-dependent manner (Fig. 2C), suggesting that UP1 partially unfolded the non-B structure of CGG16 without KCl.

The oligonucleotide CGG7 forms a slowly migrating electrophoretic species after incubating with 300 mM KCl at 4 °C overnight and subsequent diluting by 30-fold to a concentration of 10 mM KCl (Fig. 3 lane 2). The slowly migrating band disappeared by denaturing at 95 °C for 2 min (Fig. 3 lane 1). The addition of UP1 converts this slowly migrating band to the fast migrating band for the single-stranded monomolecular form (Fig. 3 lane 3). This data indicates that UP1 can dissolve a non-B structure of d(CGG)$_7$ repeats with slow mobility. Increase of the positive CD peak of CGG7 at 280 nm by addition of GST-UP1 (Fig. 2A) may indicate the conversion of this non-B structure with slow mobility into a B-form structure.

Abrogation of DNA synthesis arrest by UP1 on a single-stranded template containing d(CGG)$_{16}$

Several reports stressed that the d(CGG)$_n$ repeats on the template block DNA synthesis both *in vivo* and *in vitro* (Kang *et al.* 1995; Usdin & Woodford 1995; Samadashwily *et al.* 1997; Kamath-Loeb *et al.* 2001). Because UP1 was proved to abrogate DNA synthesis arrests on d(TTAGGG)$_n$ and d(GGCAG)$_n$ templates (Fukuda *et al.* 2002), the effect of UP1 on DNA synthesis at d(CGG)$_n$ *in vitro* was examined. A synthetic 92-mer oligonucleotide pSubCGG16 containing a d(CGG)$_{16}$ repeat was used as a template for the primer extension reaction at 15 mM KCl (Fig. 4A). DNA synthesis was obstructed within the d(CGG) repeats (Fig. 4B lane 1). As we expected, addition of a 75-fold molar excess of GST-UP1 over the template reduced the arrest of DNA synthesis *in vitro* and enhanced the full length (92 nt)

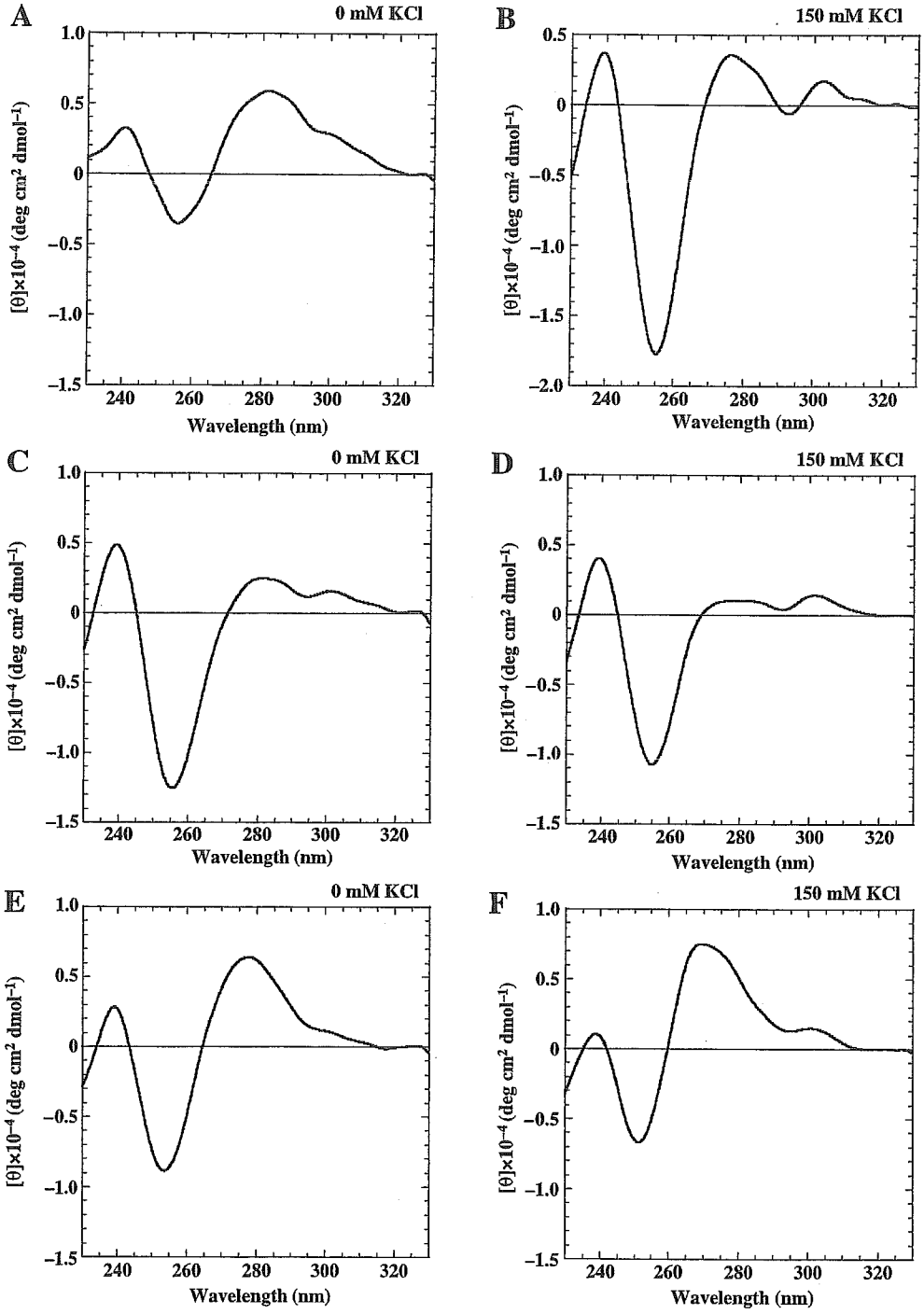

Figure 1 CD spectra of d(CGG) repeats. CD spectra of CGG7 (A, B), CGG16 (C, D), and CGG16mut (E, F) in the absence of KCl (A, C, E) and presence of 150 mM KCl (B, D, F). The concentrations of each oligonucleotide are 5.64 μM (A, C, E), 9.94 μM (B, D, F).

DNA synthesis (Fig. 4B lane 3). On the other hand, addition of GST did not have an obvious effect on the arrest of DNA synthesis, although GST subtly enhanced DNA polymerase progression itself at high concentrations (~400 μM) (data not shown). This may reflect an effect of the GST protein to stabilize DNA polymerase. Experiments using a human DNA polymerase α (pol α) gave similar results, although pol α paused more preferentially

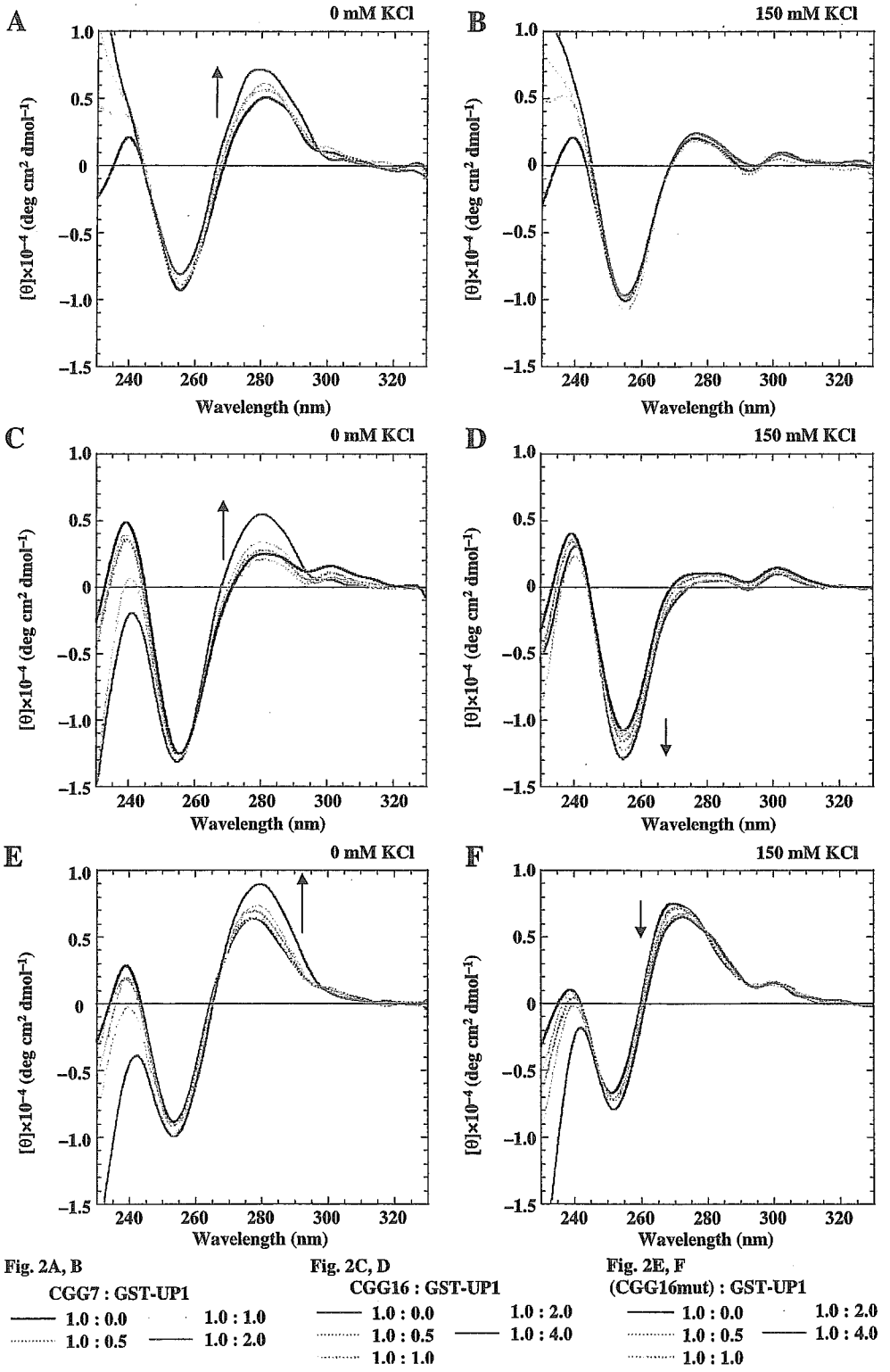

Figure 2 CD spectra showing effects of UP1 on secondary structures of d(CGG) repeat. (A) CGG7 titrated with GST-UP1 in the absence of KCl (A) and in the presence of 150 mM KCl (B). CGG16 with GST-UP1 at 0 mM KCl (C) and at 150 mM KCl (D). CGG16mut with GST-UP1 at 0 mM KCl (E) and at 150 mM KCl (F). From each spectrum, the spectrum of the corresponding protein is subtracted. Arrows indicate the changes of positive or negative peaks of CD spectra as the concentration of the added GST-UP1 increased.